COPY NO. 2

TECHNICAL REPORT 4116

NON-GREY ABSORPTION MODELS OF ABLATOR VAPORS AT HIGH TEMPERATURES WITH APPLICATION TO HYPERSONIC FLOW FIELDS

BY
HENRY E. HUDGINS, JR.

APRIL 1971

PICATINNY ARSENAL
DOVER, NEW JERSEY

UNCLASSIFIED

Security Classification

DOCUMENT CONTROL DATA - R & D

(Security classification of title, body of abstract and indexing annotation must be entered when the overall report is classified)

1. ORIGINATING ACTIVITY (Corporate author) Picatinny Arsenal, Dover, N. J.	2a. REPORT SECURITY CLASSIFICATION UNCLASSIFIED 2b. GROUP

3. REPORT TITLE
NON-GREY ABSORPTION MODELS OF ABLATOR VAPORS AT HIGH TEMPERATURES WITH APPLICATION TO HYPERSONIC FLOW FIELDS

4. DESCRIPTIVE NOTES (Type of report and inclusive dates)

5. AUTHOR(S) (First name, middle initial, last name)
Henry E. Hudgins, Jr.

6. REPORT DATE APRIL 1971	7a. TOTAL NO. OF PAGES 107	7b. NO. OF REFS 82
8a. CONTRACT OR GRANT NO. b. PROJECT NO. c. AMCMS Code 5913.21.10287 d.	9a. ORIGINATOR'S REPORT NUMBER(S) 9b. OTHER REPORT NO(S) (Any other numbers that may be assigned this report) Technical Report 4115	

10. DISTRIBUTION STATEMENT
Approved for public release; distribution unlimited.

11. SUPPLEMENTARY NOTES	12. SPONSORING MILITARY ACTIVITY

13. ABSTRACT

A representation of the "exact" spectral absorption coefficients due to the atomic continua and molecular bands of typical ablators containing C, H, O, and Si was constructed. This representation then was fitted by a multi-band model using 12 bands between $h\nu$ = 0.1 and 24.4 eV. The band model permits much more rapid calculation in applications than an "exact" model, while retaining the non-grey characteristics of the actual absorption coefficient with good accuracy as shown by various comparisons. The effect of the large uncertainties in the molecular f-numbers is investigated and found to be significant for $h\nu < 10$ eV at temperatures below about 15000° to 10000° K at pressures from 10 to 0.1 atmospheres. Spectral absorption coefficients and Planck and Rosseland mean absorption coefficients for carbon phenolic are also presented for a range of pressures from 0.1 to 10.0 atmospheres at temperatures from sublimation to 18000° K. Instructions for the utilization and application of the model are provided.

DD FORM 1 NOV 68 1473 REPLACES DD FORM 1473, 1 JAN 64, WHICH IS OBSOLETE FOR ARMY USE.

UNCLASSIFIED

Security Classification

14 KEY WORDS	LINK A		LINK B		LINK C	
	ROLE	WT	ROLE	WT	ROLE	WT
Ablator vapor absorption						
Radiating hypersonic flow fields						
Absorption models						
"Exact" spectral absorption coefficients						
Band absorption models						
f-Numbers						
Rosseland's mean absorption coefficient						
Planck's mean absorption coefficient						
Molecular band radiation						
Atomic continuum radiation						
Radiation coupled ablation						
Massive ablation						
Stagnation point ablation						
Conical body ablation						
Line radiation						
Differential approximation						

Technical Report 4116 AMC-8-70(TN)

NON-GREY ABSORPTION MODELS OF ABLATOR VAPORS AT HIGH TEMPERATURES WITH APPLICATION TO HYPERSONIC FLOW FIELDS

by

Henry E. Hudgins, Jr.

April 1971

AMCMS Code 5913.21.10287

Engineering Sciences Laboratory
Feltman Research Laboratories
Picatinny Arsenal
Dover, N. J.

PREFACE

The study presented in this report forms a part of the AMC ABM Blast Vulnerability and Survivability Program, Subtask AB-024.

A portion of this work was also submitted to the Polytechnic Institute of Brooklyn in partial fulfillment of the requirements for the degree of Master of Science (Mechanical Engineering) under the sponsorship of the Feltman Research Laboratories, Picatinny Arsenal.

TABLE OF CONTENTS

Tables

Figures

NOMENCLATURE

A	$1 + y/R_N$
$\tilde{a}$	Constant, 7.25×10^{-16} cm^2 eV^2
c	Speed of light
E_n	Integro-exponential function of order n
f	Absorption oscillator strength
H	Total enthalpy, $h + \frac{u^2 + v^2}{2}$
h	Planck's constant or static enthalpy
$h\nu$	Frequency in energy units
I	Radiative intensity
j	Power of r in continuity equation
K_P	Planck mean absorption coefficient
K_R	Rosseland mean absorption coefficient
k	Boltzmann's constant
ℓ	Reference length
M_∞	Flight Mach number
N	Number density
p	Pressure
$\vec{q}^R$	Radiative energy flux
R	Universal gas constant

R_N	Radius of curvature of body
r	Vertical distance from axis of symmetry
s	Arc length
T	Absolute temperature
t	Dummy variable of integration
u	x-component of velocity
v	y-component of velocity
x	Distance measured along body
y	Distance measured normal to body
Z	Compressibility

Greek Letters

α	Emission-corrected absorption coefficient of ablator
α'	Absorption coefficient of ablator
ΔH_{eff}	Effective heat of ablation
δ_e	Stand-off distance
ϵ_I	Ionization energy , eV
ϵ_T	Threshold energy, eV
Γ	Statistical weight factor
θ	Incidence angle, or temperature in energy units, kT, eV
λ	Wavelength

ν	Frequency
ξ	Non-hydrogenic correction factor
ρ	Density
$\sum$	Partition function
σ	Stefan-Boltzman constant
τ	Optical depth

Subscripts

a	Ablator
e	At contact surface or edge of source
i	i^{th} frequency band
k	k^{th} species
∞	Free stream
s	Shock conditions
w	Wall condition
x	External source
λ , ν	Spectral

Superscripts

C	Convective
R	Radiative
_	Nondimensional

BLANK PAGE

ABSTRACT

A representation of the "exact" spectral absorption coefficients due to the atomic continua and molecular bands of typical ablators containing C, H, O, and Si was constructed. This representation then was fitted by a multi-band model using 12 bands between $h\nu = 0.1$ and 24.4 eV. The band model permits much more rapid calculation in applications than an "exact" model, while retaining the non-grey characteristics of the actual absorption coefficient with good accuracy as shown by various comparisons. The effect of the large uncertainties in the molecular f-numbers is investigated and found to be significant for $h\nu < 10$ eV at temperatures below about 15000^{o} to 10000^{o}K at pressures from 10 to 0.1 atmospheres. Spectral absorption coefficients and Planck and Rosseland mean absorption coefficients for carbon phenolic are also presented for a range of pressures from 0.1 to 10.0 atmospheres at temperatures from sublimation to 18000^{o}K. Instructions for the utilization and application of the model are provided.

INTRODUCTION

Problem Statement

The nature of the flow about ablating bodies when radiation is important is strongly coupled to the radiative properties of the ablator vapors. This effect on the flow is produced by the momentum of the ablator vapors. The thickness of the ablator layer is related to this quantity directly (Ref 1 through 5). The ablator momentum at the wall is given by:

$$\rho_w v_w = \frac{q_w^R + q_w^C}{\Delta H_{eff}} \qquad (1)$$

where q_w^R and q_w^C are the radiative and convective heat fluxes at the wall and ΔH_{eff} is an effective heat of ablation. Thus, when q_w^R becomes important in comparison with q_w^C, the radiation flux contributes to the ablator layer thickness. This, however, is a coupled problem, since the thickness of the layer affects the value of q_w^R.

Furthermore, the air shock layer properties will be affected by the ablator layer variations and these two layers become coupled. Indeed, in the viscous diffusing analysis, the distinction is lost and the whole shock layer must be analyzed as one. Thus, we see the ablator-radiative properties which determine q_w^R become a significant property (Ref 6 through 20).

The current difficulties in defining the radiative properties of ablators are that many existing models have been specialized to specific temperature ranges by ignoring certain species, and that the "exact" calculations, although feasible, are so time-consuming, even on a high-speed computer, as to be of little practical use (Ref 11, 15, 17, 18, 19, 20).

It is the objective of this study to develop a band model for ablator vapors which will include all important species from 3000° to $20,000^{\circ}K$ and provide both useful accuracy and speed of computation.

Background

The complications caused by introducing thermal radiation into the fluid dynamics of flow fields about supersonic bodies could be ignored during the early efforts to develop suborbital vehicles such as IRBMs and ICBMs and even earth orbital re-entry vehicles, since the shock layers were relatively cool and thin.

The need to consider radiative effects first arose in designing for re-entry at superorbital velocities. Rough estimates gave early indications that radiative heat transfer could easily exceed the convective heat transfer at the stagnation point (Ref 21 - 24). Most of the work performed to date has been in this area of flight velocities so high that the radiation of the shock layer itself is the source of radiation.

However, interceptor missiles present a different problem. They fly, typically, in the Mach number range of 3 to 10 and at altitudes where radiation from the air shock layer could be neglected. But they could also be subjected to high-temperature thermal radiation from external sources, and therefore the surface heat flux can reach levels high enough to induce massive ablation.

The evolution of our understanding and the complexity of the models employed in the area of shock layers with radiation has been most excellently reviewed by Anderson (Ref 25). This development is best described by the following block diagram.

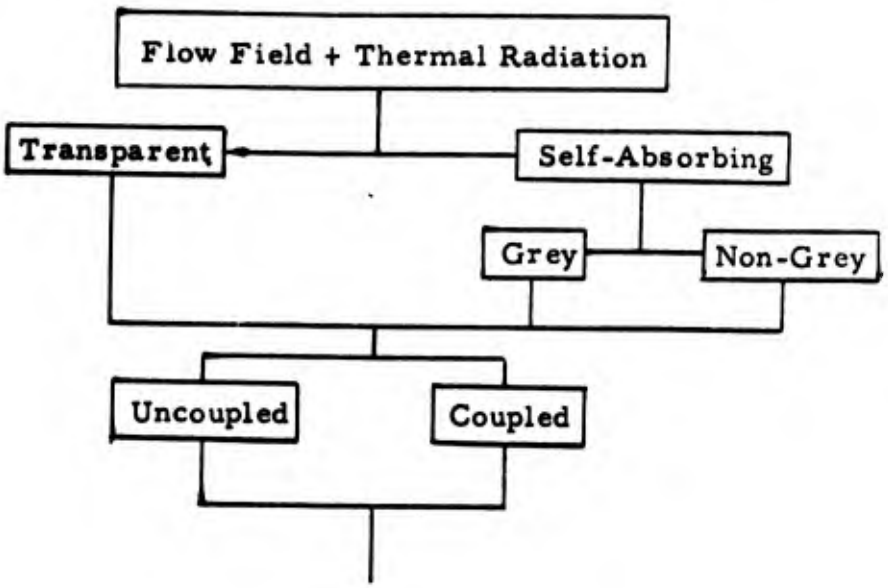

In addition, the non-grey block may be further broken down into the areas shown below.

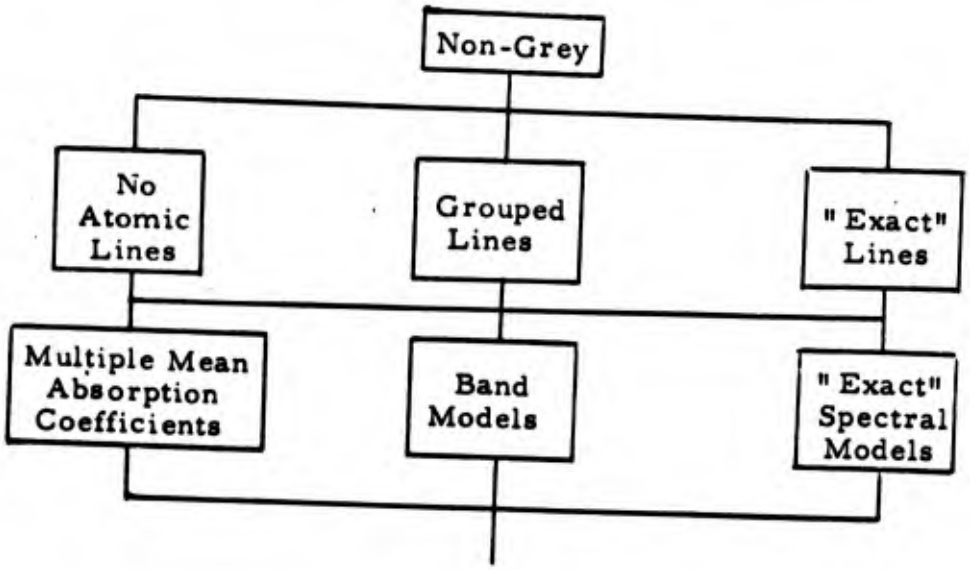

Finally, we can also divide the flow field aspect into the two catagories of ablating and nonablating; both of which have been analyzed as inviscid or viscid by various workers in the field.

Most of the work to date has assumed local thermodynamic and chemical equilibrium. Some work in the area of non-equilibrium radiation has been done, e.g., Ref 26 and 27; but as Anderson (Ref 25) points out, the conditions which make radiation important, i.e., high velocities and low altitudes, also promote equilibrium shock layer conditions.

In this study we consider the models set up of the non-grey absorption characteristics of ablator vapors, as required to compute the non-grey radiation effects in flow fields about ablating supersonic bodies.

ANALYSIS

Absorption Coefficients of Ablator Vapors

A number of non-grey absorption models for ablator vapors have been proposed in the literature (Ref 11, 15, 17, 18, 19, 20). These models cover all the non-grey possibilities discussed earlier. It also appeared than none of these models included all of the important species over the temperature range of 3000° to $20,000^{\circ}$K, which include the multi-band models as discussed by Chin (Ref 18) and the model used by Wilson and Hoshizaki (Ref 20).

In the Wilson and Hoshizaki model the atomic continua were based on the work of Biberman et al (Ref 28) and Wilson and Nicolet (Ref 29). The molecular contributions of C_2, H_2, and CO were approximately accounted for as in Hoshizaki and Lasher (Ref 15).

The multi-band models used molecular absorption values derived from the work of Weisner (Ref 30). Weisner's work was in turn based on the data and references summarized in Table 1. The cited multi-band models ignored the contributions of atomic hydrogen and carbon in the lower frequency bands, and they ignored atomic oxygen in all bands. On the other hand, Wilson's model treated the atomic continua completely, but ignored such strong molecular absorbers as C_3 and C_2H.

However, wall temperatures from 3500° to 4300°K are typical of high temperature ablators, and molecular species would always appear to be important at such temperatures, Furthermore, Chin (Ref 18) shows that a large portion of the ablator layer is very close to the wall temperature.

This is demonstrated by the results presented in Table 2, using Wilson's model after the addition of C_3 and C_2H absorption estimates. (Dominance based on absorption coefficient, not absorption cross-section.) It should be noted that these results also verify that atomic oxygen becomes an important absorber and should be accounted for. Therefore, the atomic continua model in Reference 20 was coupled with a more exact estimate of molecular absorption. The model in Reference 20 is outlined briefly below for completeness.

The approximate relations derived by Biberman and Norman (Ref 28) for photoionization from excited states and the tabulation of Wilson and Nicolet (Ref 29) for photoionization from low-lying states were used to obtain the continuum coefficients of neutral and ionized atoms. The absorption due to free-free transitions was estimated by the hydrogenic approximation.

The atomic constants used are given in the table below.

Species (k)	$(\varepsilon_I)_k$ eV	$(\varepsilon_T)_k$ eV	Γ_k
H	13.6	0.80	1
C	11.26	3.78	1.33
C^+	24.4	14.9	0.333
O	13.61	4.25	0.888
O^+	35.1	20.4	4.50

Note that in this model (Ref 20) the statistical weight factor Γ_k is defined as a constant equal to $2g_{II}/g_I$ (where g_{II} is the ground state statistical weight of the residue ion and g_I the ground state statistical weight of the parent atom.) This was changed from the definition in Reference 28 of the ratio of the temperature dependent partition functions of parent atom and residual ion, because doing so produced a better fit to the detailed data of Reference 29.

As an example of the model, the spectral absorption coefficient for O is shown here:

$$0 < h\nu < 4.25 \text{ eV}$$

$$(\alpha'_o)_1 = \frac{N_o \tilde{a} \theta \Gamma_o}{\nu^3} e^{-(\varepsilon_{I_o} - h\nu)} \xi(h\nu) \qquad (2)$$

$$4.25 \leq h\nu < 13.36 \text{ eV}$$

$$(\alpha'_o)_2 = (\alpha'_o)_1 \, e^{-(h\nu - \varepsilon_{T_o})/\theta} \qquad (3)$$

$$h\nu \geq 13.36$$

$$(\alpha'_o)_3 = (\alpha'_o)_2 + 3.6 \times 10^{-17} \frac{N_o}{\Sigma_o} \qquad (4)$$

The model for molecular absorption was set up by fitting curves to the published results of Weisner (Ref 30) filled in by data from Golden (Ref 31), Spindler (Ref 32), and Main and Bauer (Ref 33) where needed. No attempt was made to follow every minor variation in the above results. First and second order polynomials were fitted sectionally with temperature variations accounted for by second order polynomials where the temperature effect was significant.

The molecular bands and their range are summarized in Table 3. The probable range of the f-number uncertainties as reported by Weisner, normalized to Weisner's nominal values, is shown next in Table 4. Thus, this factor can be studied for its effect on the overall absorption coefficient.

The number density as a function of pressure and temperature is required to compute an absorption coefficient. The number densities used in this study are numerical results obtained from a thermochemical equilibrium computer code, FEMP, which computes equilibrium composition by minimizing the free energy function at the given temperature and pressure (see Fig 1 through 3 for data used in this study).

The absorption model discussed so far includes molecular bands and atomic continua, but does not include atomic lines. The reasons for that omission are discussed below in detail.

Theory and experiment agree that for an isothermal plasma the contribution of atomic lines to radiative heat transfer is about equal to the atomic continuum contribution (Ref 28, 34 through 40). In a non-adiabatic radiating shock layer, however, the contribution of atomic lines is reduced by radiative cooling and non-grey self-absorption. In this, Coleman (Ref 41), Page (Ref 42), Wilson (Ref 20) and Rigdon et al (Ref 17) are in qualitative agreement. There is, however, considerable disagreement as to the exact magnitude of the atomic lines contribution.

The basic computational difficulty is that including the effect of lines in an exact "line-by-line" manner is extremely costly and time-consuming even on a high-speed computer. Rigdon et al (Ref 17) performed only one viscid ablating stagnation point calculation in which the radiative, thermal, and transport properties of the ablator were all modeled exactly.

Wilson and Hoshizaki (Ref 20) attempted to simplify the line energy transfer by the grouping of lines. However, as they themselves and also Rigdon et al (Ref 17) pointed out, line-grouping is not valid when the elemental composition varies significantly across the layer thickness unless there is strong overlapping of the lines of the different species. For example, in an ablator/air shock layer there is a strong variation, and the lines are usually isolated and grouping becomes invalid (Ref 20).

Chin (Ref 18) also has proposed a line transport model for an inviscid air/ablator shock layer using only N and O lines.

Rigdon et al (Ref 17) have compared their "line-by-line" results with Wilson's and Hoshizaki's (Ref 20) " continuum only" results, and Chin's (Ref 18) "N and O lines only" results for a massive ablation case using carbon phenolic as the ablator in Figure 9 of Reference 17. The parameter compared is the radiative heat flux at the wall.

These comparisons can be briefly summarized as:

1. Rigdon's results lie about 30% above Wilson's,

2. Chin's results lie about 10% below Wilson's,

3. Rigdon, Wilson, and Chin used different models for the molecular bands and the atomic continua.

In the light of this comparison and the previous discussion of the molecular bands and the atomic continua, it was concluded that due to:

1. the inability of any current line models to agree better with themselves than with a continuum only model (when considering the ablating stagnation point problem),

2. the differing molecular band and atomic continua models employed with the different line models,

3. the already noted improvements made in this study to the atomic continua in Chin's model and to the molecular bands in Wilson's model,

it is both desirable and useful to limit this investigation to the improved continuum and band model first discussed and also study the effect of uncertainties in the molecular f-numbers.

Recent work by Olstad (Ref 43), Callis (Ref 44), and Page (Ref 42) comparing "exact" continuum and line models for air with various simplified band models had shown that in this fashion good results can be achieved for the radiating shock layer. Certainly, a similar effort devoted to developing an engineeringly useful model for ablation products which would account for atomic lines is a desirable extension of this current effort. It can be pursued once this study has clarified the contribution, clearly more important than that for air, of molecular absorption, especially near the cold wall.

Multi-band Model of Absorption

These atomic continuum and molecular band models were combined to give an "exact" model of the spectral absorption cross section of ablator vapors. This was then converted to an absorption coefficient using the number densities from FEMP for each species. This model then was used as the standard to which a multi-band model of 12 bands was fitted using an integrated average of the exact results for absorption coefficient in each band at a given temperature and pressure. Temperature effects on the absorption cross section, as distinct from its effect on absorption coefficient through number density, were curve-fitted as shown in Table 5 using forms similar to those in the band models discussed by Chin (Ref 18).

The computer code version of the 12-band model developed in this study, ABSORB, computes both the uncorrected and the induced-emission-corrected absorption coefficients using:

$$\alpha_\nu = \alpha'_\nu (1 - e^{-h\nu/kT}) \tag{5}$$

in the averaged form for the i^{th} band of:

$$\alpha_i = \alpha'_i \left[1 + \frac{kT}{(\Delta h\nu)_i} \left(e^{-(h\nu_i + \Delta h\nu_i)} - e^{-(h\nu_i)} \right) \right] \tag{6}$$

Planck and Rosseland Mean Absorption Coefficients

The Planck and Rosseland means are the two most widely used mean absorption coefficients. The former usually is considered valid in the optically thin limit, the latter in the optically thick limit. However, ways of covering the whole range of optical thicknesses by combining them have been suggested (Ref 3, 46 through 50).

It is therefore of general utility to compute these two means for ablator vapors. The Planck mean is defined as:

$$K_P = \frac{\int_{\nu=0}^{\infty} \alpha_\nu e_{b_\nu} \, d\nu}{\int_{\nu=0}^{\infty} e_{b_\nu} \, d\nu} \tag{7}$$

and the Rosseland mean as:

$$K_R = \frac{\int_{\nu=0}^{\infty} \frac{\partial e_{b_\nu}}{\partial T} \, d\nu}{\int_{\nu=0}^{\infty} \frac{1}{\alpha_\nu} \frac{\partial e_{b_\nu}}{\partial T} \, d\nu} \tag{8}$$

where

$$e_{b_\nu} = \frac{2\pi h \nu^3}{c^2} \left(e^{h\nu/kT} - 1\right)^{-1} \qquad (9)$$

The evaluation of these mean coefficients is greatly eased by the use of a band model, since within each band α_ν is a constant and the functions

$$\int_{\nu_i}^{\nu_i + \Delta\nu_i} e_{b_\nu} \, d\nu$$

and

$$\int_{\nu_i}^{\nu_i + \Delta\nu_i} \frac{\partial e_{b_\nu}}{\partial T} \, d\nu$$

need be evaluated only once for all applications.

In the computer code, ABSORB, developed for this study, this is done by means of curve-fitting the integrals.

Numerical Methods

The listing of the computer program, ABSORB, in Appendix A should be consulted for details. However, the general approach will be described here.

The need for tables of the integrated Planck function can be removed. Since the Planck function is closely approximated by Wein's law for small $n\lambda T$,

Wein's Law: $(n = 1)$

$$\frac{e_{b_\chi}}{\sigma T^5} = \frac{6.9253 \times 10^{16}}{(\lambda T)^5} e^{-25896/\lambda T} \qquad (10)$$

where $\lambda T = \mu^{o}R$, (micron-degree Rankine)

The accuracy of fit is better than 1% up to $\lambda T = 5500\ \mu^{o}R$.

Integrating:

$$\frac{e_b(0 - \lambda T)}{\sigma T^4} = \frac{6.9253 \times 10^{16}}{(25896)^4} e^{-25896/\lambda T} \left[\left(\frac{25896}{\lambda T}\right)^3 + 3\left(\frac{25896}{\lambda T}\right)^2 + 6\left(\frac{25896}{\lambda T}\right) + 6 \right] \qquad (11)$$

and the accuracy of fit is better than 1% up to $\lambda T = 7400\ \mu^{o}R$.

Above $\lambda T = 7400$ we use a curve-fit to the tabulated integral of the form:

$$\frac{e_b(0 - \lambda T)}{\sigma T^4} = (1 - a\, e^{b\lambda T})^n \qquad (12)$$

When:

$$a = 2.231$$

$$b = 1.473 \times 10^{-4}$$

$$n = \frac{1}{2}$$

the curve-fit contains less than 1% error over the range $7400 < \lambda T < \infty$, $\mu^{o}R$. It is incorporated in subroutine PLANCK of ABSORB.

The integral required to compute the Rosseland mean is:

$$I_{R_i} = \int_{\nu_i}^{\nu_i + \Delta\nu_i} \frac{\partial e_{b_\nu}}{\partial T} d\nu \qquad (13)$$

where

$$\frac{\partial e_{b_\nu}}{\partial T} = \frac{1}{2\pi k} \left(\frac{c\, e_{b_\nu}}{\nu T}\right) e^{h\nu/kT} \qquad (14)$$

Equation 13 was integrated numerically and the results curve-fitted. When $X_1 = h\nu_i$ and $X_2 = h\nu_i + \Delta h\nu_i$:

$$0 < h\nu < 3.7$$

$$I_R = 0.3343(X_2^3 - X_1^3) - 0.01354(X_2^5 - X_1^5) +$$

$$- 3.980\times10^{-3}(X_2^6 - X_1^6) + 2.203\times10^{-3} ($$

$$X_2^7 - X_1^7) - 2.567\times10^{-4}(X_2^8 - X_1^8) \qquad (15)$$

$$h\nu > 3.7$$

$$I_R = e^{-X_1}(X_1^4 + 4X_1^3 + 12X_1^2 + 24X_1 + 24) +$$

$$- e^{-X_2}(X_2^4 + 4X_2^3 + 12X_2^2 + 24X_2 + 24) \qquad (16)$$

These curve-fits are incorporated into subroutine ROSSEL in the ABSORB code.

APPLICATIONS

Clearly, the absorption model can be used for any one of its components in many situations; but it was developed as a model for high-temperature ablators. Thus, its most direct use is in flow fields about supersonic ablating bodies with radiation coupling.

The literature on this subject is expanding rapidly but the key papers to date appear to be Reference 6 through 20, 43 and 44. Various simplifying assumptions are, of course, made to reduce the full axi-symmetric Navier-Stokes equations to something more tractable, such as the Prandtl boundary layer equations, the thin shock layer approximation (Ref 45), and that the flow is inviscid.

Inviscid flow is actually achieved during massive ablation. That is, when the boundary layer is "blown off" by the momentum of the ablator vapor and viscous effects are then restricted to a contact surface between an air shock layer and an ablator layer.

Calculations made in the course of this study at the stagnation point indicate that the conditions of

1. a thin shock layer, $\delta << R_N$,
2. massive ablation, $\rho_w v_w / \rho_\infty v_\infty \geq 0.10$,
3. a cool air shock layer with respect to an external radiation source with an effective temperature of 6000° to $15000^{\circ}K$

cannot be mutually satisfied. Such a problem requires that at least the thin shock layer restriction be dropped, since it does not remain thin with both massive ablation and the moderate hypersonic free flight Mach numbers ($3 < M_\infty < 8$) required for a relatively cool air shock layer.

For the non-thin massive steady ablation case with a cool air shock layer, the required ablation layer equations would be in body-oriented orthogonal curvilinear coordinates:

Continuity

$$\frac{\partial}{\partial x}(\rho u r^j) + \frac{\partial}{\partial y}(A \rho v r^j) = 0 \qquad (17)$$

(j = 0 for 2-D, j = 1 for axisymmetric flow)

x-Momentum

$$\rho u \frac{\partial u}{\partial x} + A \rho v \frac{\partial u}{\partial y} + \frac{\rho u v}{R_N} + \frac{\partial p}{\partial x} = 0 \qquad (18)$$

y-Momentum

$$\rho u \frac{\partial v}{\partial x} + A \rho v \frac{\partial v}{\partial y} - \frac{\rho u^2}{R_N} + A \frac{\partial p}{\partial y} = 0 \qquad (19)$$

Energy

$$\rho u \frac{\partial H}{\partial x} + A \rho v \frac{\partial H}{\partial y} + A \nabla \cdot \vec{q}_R = 0 \qquad (20)$$

where

$$A = 1 + y/R_N$$

$$H = h + \frac{u^2 + v^2}{2}$$

and the geometry is made clear in the sketch below, while the equation of state may often be written:

$$p = Z \rho R T \qquad (21)$$

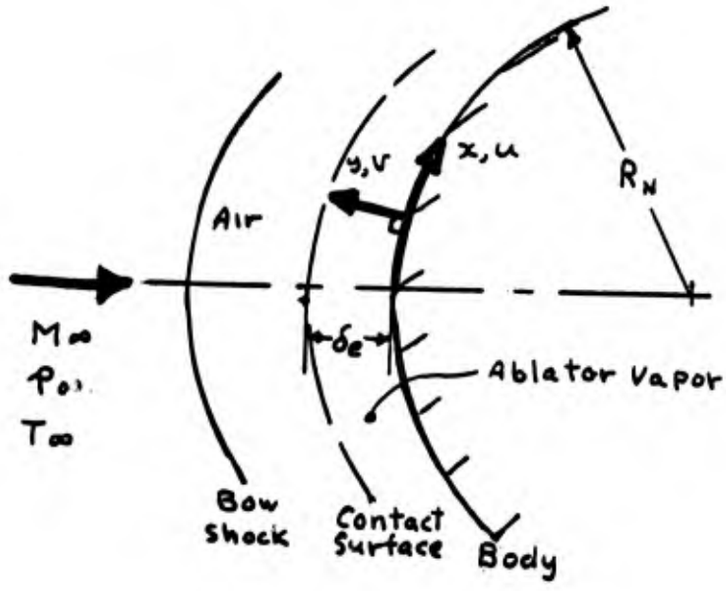

The boundary conditions in the ablation layer are:

at $y = 0$

$$\rho v = \rho_w v_w = \frac{q_w^R}{\Delta H_{eff}}$$

$$\frac{d(\rho v)}{dy} = 0$$

$$H = H_w$$

at $y = \delta_e$

$$\rho v = 0$$

$$u = u_{\delta_e}$$

$$p = p_{\delta_e}$$

In any application where radiation pressure is negligible the radiation term enters directly only into the energy equation in the form of the divergence of the radiative flux, $\nabla \cdot \vec{q}_R$. In the plane layer approximation, often used (and often justifiable), this reduces to dq^R/dy.

The development in Appendix B for an ablating stagnation point shows that the evaluation of dq^R/dy converts the differential equation (partial or ordinary) into an integro-differential equation.

The band model developed here greatly facilitates the evaluation of the integrals.

The key to the problem lies in evaluating the term

$$I_Q = \int_{\nu=0}^{\infty} \alpha_\nu \int_0^{\tau_{0,\nu}} e_{b_\nu} E_1 (|\tau_\nu - t_\nu|) \, dt_\nu \qquad (22)$$

When formulated as an N-band model we can write the term, after Callis (Ref 44), as

$$I_Q = \sum_{i=1}^{N} \alpha_i \int_0^{\tau_{0,i}} \int_{\Delta\nu_i} e_{b_\nu} E_1 (|\tau_i - t_i|) \, dt_i \qquad (23)$$

since

$$\tau_i = \int_0^y \alpha_i (y') \, dy' \tag{24}$$

which may be integrated by standard numerical quadrature routines.

If we write

$$T^{*4} = \int_{\Delta \nu_i} eb_\nu \, d\nu \tag{25}$$

then integrating Equation 22 by parts, and evaluating $dT^*/d\tau$ as a local constant, I_Q may be expressed at the k^{th} point in the mesh as*

$$I_Q = \sum_{i=1}^{N} (\alpha_i)_k \left(2T^{*4}_{i,k} - T^{*4}_{i,1} E_2(\tau_{i,k}) + \right.$$

$$- (T^{*4}_{i,M+1}) E_2(|\tau_{i,M+1} - \tau_{i,k}|) + \tag{26}$$

$$- \sum_{j=1}^{M} \left\{ \frac{(T^{*4}_{i,j+1} - T^{*4}_{i,j})}{\Delta t_i} \left[E_3(|t_{i,j+1} - \tau_{i,k}|) + \right. \right.$$

$$\left. \left. - E_3(|t_{i,j} - \tau_{i,k}|) \right] \right\} \Bigg)$$

with

$$\Delta t_i = \tau_{i,j+1} - \tau_{i,j} . \tag{27}$$

---

*Note that this device has eliminated the need to deal with E_1 which has a logarithmic singularity at 0.

The problem is often further simplified by the exponential kernel approximation

$$E_n(t) = a_n e^{-b_n t} \tag{28}$$

Sparrow and Cess (Ref 48) discuss choosing the values of a_n and b_n so that the areas and first moments of $E_2(t)$ are matched over the range $0 \leq t \leq \infty$ (Lick's method). The result is:

$$E_2(t) = \frac{3}{4} e^{-3t/2} \tag{29}$$

Then from

$$E_{n+1}(t) = -\int E_n(t)\, dt \tag{30}$$

$$E_3(t) = \frac{1}{2} e^{-3t/2} \tag{31}$$

On the other hand, Chin (Ref 18) chose to match the value and slope of $E_3(t)$ at $t = 0$, yielding:

$$E_3(t) = \frac{1}{2} e^{-2t} \tag{32}$$

and

$$E_2(t) = e^{-2t} \tag{33}$$

When one is expecting the value of t to be always near zero, Chin's procedure would appear the more desirable, since Lick's procedure does not match the value of $E_2(t)$ at $t = 0$ by 25%. However, in a problem where t can assume large values, Lick's method is more accurate over the range.

Another approach that has been proposed is to eliminate the integral completely by the differential approximation for a non-grey gas. This method evolves from a grey gas approximation constructed by Vincenti and Kruger (Ref 3), Traugott (Ref 46), and Cheng (Ref 47). In vector form:

$$\left(\nabla/K \left[(\nabla \cdot \vec{q}^R)/K \right] \right. - 3\vec{q}^R + 4\pi (\nabla B/K) = 0 \qquad (34)$$

which satisfies both the optically thin and optically thick limits, since for a grey gas $K_P = K_R = K$. In fact, as Sparrow and Cess (Ref 48) point out, in the optically thick limit it is a higher order approximation than the radiation slip approach.

To go to a non-grey gas approximation, Traugott (Ref 49) requires that the approximation satisfy an opaque gas:

$$\vec{q}^R = 4\pi/3 \, (\nabla B/K_R) \qquad (35)$$

and a transparent gas

$$\nabla \cdot \vec{q}^R = -4\pi K_P B \qquad (36)$$

to yield

$$\frac{1}{K_R} \nabla \left(\frac{1}{K_P} \nabla \cdot q^R \right) - 3 q^R + \frac{4\pi}{K_R} \nabla B = 0 \qquad (37)$$

or as in Cogley et al (Ref 50)

$$\frac{1}{K_R} \nabla \left(\frac{1}{K_P} \nabla \cdot \vec{q}^R \right) - 3\vec{q}^R - \frac{16\sigma T^3}{K_R} \nabla T = 0 \qquad (38)$$

Here we have an excellent application for the Planck and Rosseland mean absorption coefficients computed in this study.

This absorption model and the planar radiation formulation can be applied to flow configurations other than a stagnation point. For example, Picatinny Arsenal already has a flow field program for the massive ablation of conical bodies with uncoupled radiation (Ref 81,82). This program is discussed in Appendix C, in which it is also shown that the planar radiation model is still applicable. The logical next step is to couple this absorption model to the flow field in this program.

RESULTS

General

The ablator spectral absorption models existing before this study have been shown to require the addition of such molecular species as C_2H and C_3 and of atomic O, the extension of the effects of atomic C and H in frequency, and a more detailed treatment of molecular species in general in order to cover the range of temperatures from 3000° to 20000° K (see Table 2). Therefore, a more detailed "exact" model of molecular band and atomic continuum absorption for C, H, O, and Si systems was developed by collecting heretofore scattered current knowledge into one package.

In applications, however, a model which can be calculated more quickly without sacrificing a great deal of accuracy is needed. Therefore, a multi-band model of 12 bands was fitted to the exact calculations (see Table 5). This band model was then coded in FORTRAN IV as a computer program, ABSORB. ABSORB computes either a 12-band uncorrected and emission-corrected spectral absorption coefficient, or a 2-band absorption model with a break point at 1100 Å and the Planck and Rosseland mean absorption coefficients.

The range of applicability of the computer program is currently limited by the neglect of atomic line radiation. When line radiation and absorption is negligible, any temperature which is above sublimation and below the neglected doubly ionized states at the given pressure can be computed for systems composed of C, H, O, and Si for a frequency range of 0.1 to 24.4 eV.

The computer program is listed in Appendix A.

Comparison of Results

The 12-band absorption model developed in this study for molecular bands and atomic continua is compared with the "exact" model calculations for pressures of 0.1, 1.0, and 10.0 atmospheres and temperatures from 3500°K to 15000°K for a carbon phenolic ablator of composition $C_{18}H_{4.3}O$. The number densities used are given in Figures 1 through 3. The agreement is quite satisfactory over the entire range of pressure, temperature, and frequency, as can be seen from Figures 4 through 15.

Molecular f-Number Uncertainties

The current state of knowledge of the absorption oscillator strengths, or f-numbers, of polyatomic molecules results in large uncertainties in the correct values. The values of the f-numbers as ascertained from the literature (Ref 18, 30 through 33) are expressed in terms of ratios of the lowest and highest values to the nominal values in Table 4.

This range of f-numbers then was used to compute the spectral absorption coefficients for a range of temperatures and pressures. The effect is shown for a pressure of one atmosphere in Figures 16 through 19. The variation of absorption coefficient with molecular f-number is seen to be quite important for frequencies below $h\nu$ = 10 eV for temperatures below 10000°K. In many applications this would be the most important part of the spectrum with regard to the peak of incident radiation.

The results at 0.1 and 10.0 atmospheres are very similar. It is clear from the results, however, that the maximum temperature at which molecular effects are still significant increases with increasing pressure. This would be expected from the number density data (see Fig 1 through 3) as the number density of molecular species becomes higher at a given temperature as pressure goes up.

The molecular band uncertainty which contributes most to this f-number variation effect can be seen to be the CO "Fourth Positive" from $h\nu$ = 3.9 to 12.4 eV, (1000 to 3200 Å) (Table 3).

Planck and Rosseland Means

The Planck and Rosseland mean absorption coefficients were also computed and are plotted in Figures 20 and 21 as a function of temperature, pressure, and f-number.

The effect of the molecular f-number uncertainties is also apparent in these integrated coefficients and the variation with temperature and pressure is perhaps even clearer in this form. The Rosseland mean is more strongly influenced than the Planck.

CONCLUSIONS

1. The 12-band molecular band and atomic continuum absorption model developed in this study represents quite closely the "exact" model compiled in this study for a range of temperatures from 3500°K to 20000°K at a pressure from 0.10 to 10.0 atmospheres.

2. Both this band model and the "exact" model include important absorbing species neglected in other models available in the literature. These include C_3, C_2H, O, and C and H at low frequencies.

3. The effect on spectral absorption coefficient of the large uncertainties in some molecular band f-numbers is significant at frequencies below 10 eV for temperatures as high as 15000°K at 10 atmospheres and 10000°K at 0.10 atmospheres. This effect remains significant in the integrated coefficients in both their Planck and Rosseland forms.

4. Now that the effect of the molecular uncertainty has been better defined, it is clear that these f-numbers need to be better determined. The band with the largest effect was the CO "Fourth Positive".

5. The logical next step is to include atomic line radiation. Since the purpose of a band model is more rapid computation, the tedious exact line calculations presently available must be replaced. Olstad (Ref 43) and Callis (Ref 44) recently have reported good results with "equivalent band" models for line radiation.

6. A number of applications of the absorption model and its results are suggested in this study. An appropriate next step would be to compare the exponential integral approximation method with the differential approximation.

REFERENCES

1. Kaatari, G., "The Effect of Simulated Ablation-Gas Injection on the Shock Layer of Blunt Bodies at Mach Numbers of 3 and 5", NASA TN D-2954, August 1965

2. Pai, S. I., Radiation Gas Dynamics, Springer-Verlag, New York, 1966

3. Vincenti, W. G., and Kruger, C. H., Jr. Introduction to Physical Gasdynamics, Wiley, New York, 1965

4. Truitt, R. W., Hypersonic Aerodynamics, The Ronald Press Co., New York, 1959

5. Cresci, R. J., and Libby, P. A., "The Downstream Influence of Mass Transfer at the Nose of a Slender Cone", Journal of Aerospace Sciences, Vol 29, No. 7, pp 815-826, July 1961

6. Wilson, K. H., "Massive Blowing Effects on Viscous, Radiating, Stagnation Point Flow", AIAA Paper No. 70-203, 8th Aerospace Sciences Meeting, New York, January 1970

7. Howe, J. T., and Viegas, J. R., "Solutions of the Ionized Radiating Shock Layer Including Reabsorption and Foreign Species Effects and Stagnation Region Heat Transfer", NASA TR-159, 1963

8. Hoshizaki, H., and Wilson, K. H., "Viscous Radiating Shock-Layer about a Blunt Body", AIAA Journal, Vol 3, No. 9, pp 1614 - 1622, September 1965

9. Wilson, K. H., and Hoshizaki, H., "Inviscid Nonadiabatic Flow about Blunt Bodes", AIAA Journal, Vol 3, No. 1, pp 67-74, January 1965

10. Anderson, J. D., "Non-gray Radiative Transfer Effects on the Radiating Stagnation Region Shock Layer and Stagnation Point Heat Transfer", Naval Ordnance Laboratory, NOLTR-67-104, July 1967

11. Dirling, R. B., Jr., Rigdon, W. S., and Thomas, M., "Stagnation-Point Heating Including Spectral Radiative Transfer", Proceedings of the 1967 Heat Transfer and Fluid Mechanics Institute, Stanford University Press, Palo Alto, California, 1967

12. Hoshizaki, H., and Wilson, K. H., "Convective and Radiative Heat Transfer During Super Orbital Entry", AIAA Journal, Vol 5, No. 1, pp 25-35, January 1967

13. Anderson, J. D., "Non-gray Radiative Stagnation Point Heat Transfer", AIAA Journal, Vol 6, No. 4, pp 758-760, April 1968

14. Anderson, J. D., "Heat Transfer from a Viscous Non-gray Radiating Shock Layer", AIAA Journal, Vol 6, No. 8, pp 1570-1573, August 1968

15. Hoshizaki, H., and Lasher, L. E., "Convective and Radiative Heat Transfer to an Ablating Body", AIAA Journal, Vol 6, No. 8, pp 1441-1449, August 1968

16. Page, W. A., Compton, D. L., Borucki, W. J., Ciffone, D. L., and Cooper, D. M., "Radiation Transport in Inviscid Non-adiabatic Stagnation Region Shock Layers", Paper 68-784, 3rd Thermophysics Conference, AIAA, June 1968

17. Rigdon, W. S., Dirling, R. B., Jr., and Thomas, M., "Radiative and Convective Heating During Atmosphere Entry", NASA CR-1170, September 1968

18. Chin, J. H., "Radiation Transport for Stagnation Flows Including Effects of Lines and Ablator Layers", AIAA Journal, Vol 7, No. 7, pp 1310-1318, July 1969

19. Rigdon, W. S., Dirling, R. B., Jr., and Thomas, M., "Stagnation Point Heat Transfer During Hypervelocity Atmospheric Entry", McDonnell Douglas Astronautics, DAC-63243, July 1969

20. Wilson, K. N., and Hoshizaki, H., "Effect of Ablation Product Absorption and Line Transitions on Shock Layer Radiative Transport", NASA CR-1264, February 1969

21. Howe, J. T., "Shielding of Partially Reflecting Stagnation Surfaces Against Radiation by Transpiration of an Absorbing Gas", NASA TR-R-95, 1961

22. Yoshikawa, K. K., and Wick, B. H., "Radiative Heat Transfer During Atmosphere Entry at Parabolic Speeds", NASA TN-D-1074, 1962

23. Allen, H. J., Seiff, A., and Winovick, W., "Aerodynamic Heating of Conical Entry Vehicles at Speeds in Excess of Earth Parabolic Speeds", NASA TR-R-185, December 1963

24. Craig, R. A., and Davey, W. C., "Thermal Radiation from Ablation Products Injected into a Hypersonic Shock Layer", NASA TN-D-1978, 1963

25. Anderson, J. D., "An Engineering Survey of Radiating Shock Layers", AIAA Journal, Vol 7, No. 9, pp 1665-1675, September 1969

26. Conti, R. J., "A Theoretical Study of Non-Equilibrium Blunt-Body Flows", Journal Fluid Mechanics, Vol 24, p 65, 1966

27. Curtis, J. T., and Strom, C. R., "Computations of the Non-Equilibrium Flow of Viscous Radiating Fluid about a Blunt Axisymmetric Body, Vol I: Equations and Results", Air Force Flight Dynamics Laboratory AFFDL TR-67-40, June 1967

28. Biberman, L. M., and Norman, G. E., "Recombination Radiation and Brehmstrahlung of a Plasma", J. Quant. Spectrosc. Radiat. Transfer, Vol 3, pp 221-245, 1963

29. Wilson, K. H., and Nicolet, W. E., "Spectral Absorption Coefficients of Carbon, Nitrogen, and Oxygen Atoms", Lockheed Missile and Space Corp., LMSC 4-17-66-5, November 1966

30. Weisner, J. D., "Hardening Technology Study, II, Vol III, Part III: Radiative Properties", Lockheed Missile and Space Corp., LMSC-B130391, September 1966

31. Golden, S. A., "Approximate Spectral Absorption Coefficients of Electronic Transitions in Diatomic Molecules", J. Quant. Spectrosc. Radiat. Transfer, Vol 7, pp 225-250, 1967

32. Spindler, R. J., "Franck-Condon Factors Based on RKR Potentials with Applications to Radiative Absorption Coefficients", J. Quant. Spectrosc. Radiat. Transfer, Vol 5, pp 165-204, 1965

33. Main, R. P., and Bauer, E., "Equilibrium Opacities and Emissivities of Hydro-Carbon-Air Mixtures at High Temperatures", J. Quant. Spect. Radiat. Transfer, Vol 7, pp 527-557, 1967

34. Allen, R. A., Textoris, A., and Wilson, J., "Measurements of the Free-Bound and Free-Free Continua of Nitrogen, Oxygen and Air", J. Quant. Spectrosc. Radiat. Transfer, Vol 5, pp 95-108, 1965

35. Nerem, R. M., and Stickford, G. H., "Shock Tube Studies of Equilibrium Air Radiation", AIAA Journal, Vol 3, No. 6, pp 1011-1019, June 1965

36. Wood, A. D., Hoshizaki, H., Andrews, J. C., and Wilson, K.H., "Measurements of the Total Radiant Intensity of Air", AIAA Journal, Vol 7, No. 1, pp 130-139, January 1969

37. Nerem, R. M., "Atomic Line Radiation in Equilibrium Air", AIAA Journal, Vol 4, No. 8, pp 1485-1486, August 1965

38. Gruszczynski, J. S., and Warren, W. R., "Study of Equilibrium Air Total Radiation", AIAA Journal, Vol 5, No. 3, pp 517-525, March 1967

39. Thomas, G. M., and Menard, W. A., "Measurements of the Continuous and Atomic Line Radiation from High Temperature Air", AIAA Journal, Vol 5, No. 12, pp 2214-2223, December 1967

40. Golobic, R. A., and Nerem, R. M. "Shock-Tube Measurements of End-Wall Radiative Heat Transfer in Air", AIAA Paper 67-695, Electric Propulsion and Plasmadynamics Conference, Colorado Springs, September 1967

41. Coleman, W. D., Hearne, L. G., Lefferdo, J. M., and Vojvodich, N. S., "A Study of the Effects of Environmental and Ablator Performance Uncertainties on Heat Shield Requirements for Blunt and Slender Hyperbolic Re-Entry Bodies", AIAA Paper No. 68-154, January 1968

42. Page, W. A., Compton, D. L., Boruchi, W. J., Ciffone, D. L., and Cooper, P. M., "Radiative Transport in Inviscid Non-Adiabatic Stagnation-Region Shock Layers", AIAA Paper No. 68-784, June 1968

43. Olstad, W. B., "Blunt-Body Stagnation-Region Flow with Non-grey Radiation Heat Transfer -- A Singular Perturbation Method", NASA TR R-295, November 1968

44. Callis, L. B., "Solutions of Blunt-Body Stagnation-Region Flow with Non-grey Emission and Absorption of Radiation by a Time-Asymptotic Technique", NASA TR R-299, January 1969

45. Hayes, W. D., and Probstein, R. F., Hypersonic Flow Theory, Academic Press, New York, 1959

46. Traugott, S. C., "A Differential Approximation for Radiative Transfer with Application to Normal Shock Structure", Proceedings of the 1963 Heat Transfer Fluid Mechanics Institute, p 1, Stanford University Press, Stanford, California, 1963

47. Cheng, P., "Two-dimensional Radiating Gas Flow by a Moment Method", AIAA Journal, Vol 3, No. 3, pp 981-982, March 1965

48. Sparrow, E. M., and Cess, R. D., Radiation Heat Transfer, Brooks/Cole Publishing Co., 1966

49. Traugott, S. C., "Radiative Heat Flux Potential for a Non-grey Gas", AIAA Journal, Vol 4, No. 3, pp 541-542, March 1966

50. Cogley, A. C., Vincenti, W. G., Giles, S. E., "Differential Approximation for Radiative Transfer in a Non-grey Gas near Equilibrium", AIAA Journal, Vol 6, No. 3, pp 551-553, March 1968

51. Mohler, F. L., "Photoionization of Atoms and Molecules", National Bureau of Standards, NBS TN-131, January 1962

52. Dunn, G. H., "Franck-Condon Factors for the Ionization of H_2 and D_2", Joint Institute for Laboratory Astro-Physics, Rpt. No. 57, December 1965

53. Soshnikov, V. N., "Optical Absorption Cross Sections in Electronic Bands of Diatomic Molecules at High Temperatures", Optics and Spectroscopy, Vol 17, pp 186, 1964

54. Anonymous, "Absolute Intensities of Electronic Transitions in Diatomic Molecules", Soviet Physics Uspekhi, Vol 4, p 425, 1961

55. Patch, R. W., "Vibrational Overlap Integrals for Ultraviolet Bands of H_2", J. Chem. Phys., Vol 41, pp 1881-1883, 1964

56. Hexter, R. M., "Evaluation of Lattice Sums in the Calculation of Crystal Spectra", J. Chem. Phys., Vol 37, pp 1347-1356, 1962

57. Meyer, V. D., Skerbele, A., and Lassettre, E., "Intensity Distribution in the Electron-Impact Spectrum of Carbon Monoxide at High Resolutions and Small Scattering Angles", J. Chem. Phys., Vol 43, pp 805-816, 1965

58. Anonymous, "Laboratory Astrophysics", J. Quant. Spectrosc. Radiat. Transfer, Vol 2, pp 433-439, 1962

59. United Aircraft, "Theoretical and Experimental Investigations of Spectral Opacities of Mixtures of Hydrogen and Diatomic Gases", United Aircraft Research Laboratories, RTD-TDR-63-1102, November 1963

60. General Electric Co., "Venus-Mars Capsule Study", Missile and Space Division, GE 100(1), Vol II, 1962

61. Robinson, D., and Nicholls, R. W., "Intensity Measurements in the O_2^+ Second Negative, CO Angstrom and Third Positive and NO γ and δ Molecular Band System", Proc. Phys. Soc., Vol 71, p 957, 1958

62. Fairbairn, A. R., "Spectrum of Shock Heated Gases Simulating the Venus Atmosphere", AIAA Journal, Vol 2, p 1004, 1964

63. National Bureau of Standards, "Franck-Condon Factors to High Vibrational Quantum Numbers III: CN", J. Research NBS, Vol 66A, pp 75-78, 1964

64. Bennett, R. G., and Dalby, F. W., "Experimental Oscillator Strength of the Violet System of CN", J. Chem. Phys., Vol 36, p 339, 1962

65. Main, R. P, and Bauer, E., "Opacities of Carbon-Air Mixtures at Temperatures from 3000° to 10000° K", Aeronutronics Corp., Pub. No. U-3046, 12 March 1965

66. Allen, C. W., Astrophysics Quant., University of London, Athlone Press, 1963

67. Jain, D. C., "Transition Probability Parameters of the Swan and Fox-Herzberg Band Systems of the C_2 Molecule", J. Quant. Spectrosc. Radiat. Transfer, Vol 4, pp 427-440 1964

68. Nicholls, R. W., "Franck-Condon Factors to High Quantum Numbers VI: C_2 Band Systems", J. Res. NBS, Vol 69A, pp 397-400, 1965

69. Clementi, E., "Transition Probabilities for Low-Lying Electronic States in C_2", Astrophysics J., Vol 132, pp 898-904, 1960

70. Branscomb, L. M., and Pagel, E. J., "Atomic and Molecular Negative Ions in Stellar Atmospheres", Monthly Notices of the R.A.S., Vol 118, pp 258-270, 1958

71. Fink, E., and Welge, K. H., "Lifetime of the Electronic States N_2 ($^3\pi u$), N_2^+ ($B^2\Sigma^+ u$), NH ($A^3\pi$), NH ($C^1\pi$), PH ($^3\pi$)", Zeit. f. Naturforsch, Vol 192, 1 1193, 1964

72. Heitler, W., "The Dissociation Energy of Hydrocarbons", J. Chem. Phys., Vol 54, pp 265-268, 1957

73. Penner, S. S., Quantitative Molecular Spectroscopy and Gas Emissivities, Addison and Wesley, Reading, Penn., 1959

74. Menzel, D. H., and Pekeris, C., "Absorption Coefficients and Hydrogen Line Intensities", Monthly Notices of the R.A.S., Vol 96, p 7, 1935

75. Bethe, H. A., and Salpeter, E. E., Quantum Mechanics of One-and Two-Electron Atoms, Academic Press, New York, 1957

76. Aller, L. H., Astrophysics: The Atmospheres of the Sun and Stars, Ronald Press, New York, 1963

77. Frank-Kamenetskii, D., "Physical Processes in Stellar Interiors", NASA TT-F-124

78. Goulard, R., "Fundamental Equations of Radiation Gas Dynamics", The High Temperature Aspects of Hypersonic Flow, W. C. Nelson, Ed., Pergamon Press, 1964

79. Goulard, R., and Goulard, M., "One-Dimensional Energy Transfer in Radiant Media", Int. Jnl. Heat. Mass Transfer, Vol 1, p 81, 1960

80. Viskanta, R., and Merriam, R. L., "Shielding Surfaces in Couette Flow Against Radiation by Transpiration of an Abosrbing-Emitting Gas", Int. J. Heat Mass Transfer, Vol 10, pp 641-653, 1967

81. T. D. Taylor, "Massive Ablation of a Cone in High Temperature Supersonic Flow", Picatinny Arsenal Technical Report 3571, June 1967

82. T. D. Taylor, "Computer Programs for Calculation of Flow Past a Finite Cone with Large Surface Mass Addition", Picatinny Arsenal Technical Report 3573, April 1968

TABLE 1

Transition probabilities for radiation absorption

Species	Process	Principal Data	Other Data (F-C Factors, etc)
H_2	Photoionization	Empirical data from Ref 51	Ref 52
H_2	Molecular continuum	Theoretical data from Ref 55	
H_2	Lyman band system	f = 0.2 from Ref 54	
H_2	Werner band system	f = 0.4 from Ref 54	Ref 55
CO	Fourth positive band system	f = 0.19 from Ref 56, 57	Ref 58, 59
CO	Asundi band system	f = 0.03 from Ref 60	
CO	Angstrom band system	f = 0.03 from Ref 60	Ref 61
CN	Red band system	f = 0.008 from Ref 62	Ref 63
CN	Violet band system	f = 0.027 from Ref 64	Ref 65
CN	D-X band system	f = 0.04 from Ref 65	
CN	D-A band system	f = 0.02 from Ref 65	
C_2	Swan band system	f = 0.029 from Ref 66	Ref 67
C_2	Fox-Herzberg band system	f = 0.05 from Ref 65	Ref 67
C_2	Freymark band system	f = 0.02 from Ref 65	Ref 80

TABLE 1 (cont'd)

Species			
C_2	Mulliken band system	f = 0.10 from Ref 65	Ref 68
C_2	Deslandres-d'Azambuja system	f = 0.10 from Ref 65	Ref 68
C_2	Phillips band system	f = 0.0038 from Ref 69	Ref 68
C_2	Photoionization	Approximate model described in Ref 30	
C_2^-	Photodetachment	Ref 70	
C_3	4050 Angstrom band system	Ref 65	Ref 71, 72
H	Photoionization	Ref 66, 73-77	

TABLE 2

Dominant absorbing species

$T = 5000^{o}K$, $p = 1$ atm

Frequency (eV)	Dominant Absorbing Species
0 to 1.8	C_2, C_2H
1.8 to 5.0	C_2
5.0 to 6.4	C_2, C_3
6.4 to 7.0	CO, H_2(weak)
7.0 to 10.0	CO
10.0 to 11.2	C, CO
11.2 to 13.6	C
13.6 to 24.4	C, CO, H

$T = 10000^{o}K$, $p = 1$ atm

Frequency (eV)	Dominant Absorbing Species
0 to 2.0	C, H(weak)
2.0 to 4.8	C, C_2, H(weak)
4.8 to 6.2	C, C_2, CO, H(weak)
6.2 to 9.6	C, CO, H(weak)
9.6 to 13.6	C
13.6 to 24.4	C, H, O(weak)

TABLE 2 (cont'd)

$T = 15000^{o}K$, $p = 1$ atm

Frequency (eV)	Dominant Absorbing Species
0 to 0.2	C, H, O(weak)
0.2 to 7.0	C, H, O
7.0 to 13.6	C
13.6 to 17.8	C, H
17.8 to 19.0	C, H, O
19.0 to 24.4	C, H, O, C^{+}

TABLE 3

Molecular bands

Species	Band	Wavelength (Å)
H_2	Photo	500 to 1400
	Werner	600 to 1400
	Lyman	1100 to 3400
CO	Photo	500 to 900
	4 +	1000 to 3200
	Asundi	6900 to 8300
C_2	Mulliken	1800 to 2300
	Freymark	2000 to 3600
	Deslandres-d'Azambuja	2000 to 5200
	Fox-Herzberg	2400 to 5200
	Swan	3000 to 124000
C_2H	Violet	2000 to 6200
	X-D	1500 to 3200
	A-D	1400 to 3200
	Red	5200 to 50000

TABLE 3 (cont'd)

Species	Band	Wavelength (Å)
C_3	4056Å	3600 to 6200
	Violet	2000 to 2500

TABLE 4

Range of molecular band f-numbers

Species	Band	f-number ratio		
		Nominal	Low	High
C_2	Swan	1.0	0.203	1.52
	F-H	1.0	0.40	4.0
	D-D	1.0	0.10	1.0
	Frey	1.0	0.10	10.0
	Mull.	1.0	0.20	2.0
CO	4 +	1.0	1.0	11.0
	Asundi	1.0	1.0	1.0
	Photo	1.0	1.0	1.0

TABLE 5

12-Band model for ablator absorption cross sections

$$\sigma = f\,\sigma_0\, e^{-B/T}$$

Band No.	Frequency, eV Lower	Upper	System	σ_0 (cm^2)	B (eV)[a]	Remarks
1	0.1	0.4	C_2 Swan[b]	1.86(-16)[c]	1.2	f = 0.029(nom)[d]
			C_2H (red)[e]	4.0(-18)	0	f = 0.008
			C continuum	1.33(-13)	11.2	f = 1.0
			Si continuum	7.04(-17)	7.18	f = 1.0
			H continuum	-	-	$\sigma_H = 1.0\times10^{-14} T\, e^{-13.2/T}$
			O continuum	-	-	$\sigma_0 \cong \sigma_H$

[a] Hence, T is in eV

[b] The C_2 Swan contribution in the far IR has been increased by a factor of 10 in the first 3 bands to account for neglected contributors in this region (Phillips, Ballick-Ramsey, etc.)

[c] (-16) = 10^{-16}

[d] The cited f numbers are those used by Weisner (Ref 30) in his calculations. Any uncertainty in these values is covered in the table of f-number ratios

[e] The C_2H contribution is obtained by analogy to the isoelectronic CN red and violet bands

TABLE 5 (cont'd)

Band No.	Frequency, eV Lower	Upper	System	σ_0 (cm^2)	B $(eV)^a$	Remarks
2	0.4	1.0	C_2Swan	1.86(-16)	1.2	f = 0.029
			C_2H (red)	4.0(-17)	0	f = 0.008
			C continuum	8.65(-15)	11.5	f = 1.0
			Si continuum	7.04(-17)	7.18	f = 1.0
			H continuum	-	-	$\sigma_H = 4.0 \times 10^{-16} T e^{-12.8/T}$
			O continuum	-	-	$\sigma \cong \sigma_H$
3	1.0	2.0	C_2Swan	1.86(-16)	1.2	f = 0.029
			C_2H (red)	4.0(-17)	0	f = 0.008
			C continuum	5.5(-16)	10.7	f = 1.0
			Si continuum	7.04(-17)	7.18	f = 1.0
			H continuum	-	-	$\sigma_H = 4.0 \times 10^{-16} T e^{-12.8/T}$
			O continuum	- -	-	$\sigma_0 \cong \sigma_H$

TABLE 5 (cont'd)

Band No.	Frequency, eV Lower	Upper	System	σ_0 (cm^2)	B (eV)	Remarks
4	2.0	3.4	C_2Swan	7.5(-17)	0	f = 0.029
			C_2F-H	3.94(-18)	0.29	f = 0.05
			C_2D-D	3.26(-18)	0.65	f = 0.06
			C_3 λ4056	7.8(-17)	0.65	f = 0.13
			C_2H (red)	1.0(-16)	0	f = 0.008
			C_2H (violet)	3.7(-17)	0	f = 0.027
			C continuum	5.9(-17)	9.55	f = 1.0
			Si continuum	2.04(-17)	6.11	f = 1.0
5	3.4	5.2	C_2Swan	3.19(-18)	0.27	f = 0.029
			C_2 F-H	2.44(-17)	0	f = 0.05
			C_2 D-D	1.31(-17)	0.79	f = 0.06
			C_2 Frey	2.41(-16)	1.52	f = 0.02
			C_2^-	3.00(-17)	0	f = 1.0
			C_2H (violet)	3.7(-18)	0	f = 0.008
			SiO A-X	2.09(-17)	0	f = 0.19
			C continuum	1.8(-17)	8.75	f = 1.0
			Si continuum	3.36(-18)	3.44	f = 1.0
			H continuum	3.38(-17)	10.2	f = 1.0

TABLE 5 (cont'd)

Band No.	Frequency, eV Lower	Upper	System	σ_0 (cm^2)	B (eV)	Remarks
6	5.2	6.8	C_2 D-D	4.5(-19)	1.17	f = 0.06
			C_2 Frey.	3.98(-16)	0.72	f = 0.02
			C_2 Mull.	1.51(-17)	0	f = 0.10
			CO 4 +	3.32(-18)	1.6	f = 0.19[f]
			H_2 Lyman	5.0(-18)	0	f = 0.20
			C_2^-	2.0(-17)	0	f = 1.0
			SiO A-X	2.40(-17)	0	f = 0.19
			C_3 (violet)	9.0(-17)	0	f = 0.05
			C continuum	8.9(-18)	8.35	f = 1.0
			Si continuum	1.69(-17)	2.63	f = 1.0
			H continuum	1.19(-17)	10.2	f = 1.0
7	6.8	3.6	CO 4 +	5.5(-18)	0	f = 0.19
			H_2 Lyman	1.25(-17)	0	f = 0.2
			C continuum	3.2(-18)	3.77	f = 1.0
			Si continuum	7.61(-17)	0.952	f = 1.0
			H continuum	3.09(-18)	2.67	f = 1.0

[f]There is an ambiguity in the literature as to whether Weisner used f = 0.19 or 0.017. Hence, the high f-ratio is 11.2

TABLE 5 (cont'd)

Band No.	Frequency, eV Lower	Upper	System	σ_0 (cm^2)	B (eV)	Remarks
8	8.6	10.0	CO 4 +	6.00(-18)	0	f = 0.19
			H_2 Lyman	1.25(-17)	0	f = 0.2
			C continuum	3.9(-18)	2.86	f = 1.0
			Si continuum	3.34(-18)	0.177	f = 1.0
			H continuum	3.09(-18)	10.2	f = 1.0
9	10.0	11.2	CO 4 +	5.65(-19)	0.46	f = 0.19
			H_2 Lyman	1.25(-17)	0	f = 0.2
			C continuum	8.2(-18)	1.18	f = 1.0
			Si continuum	3.34(-18)	0.87	f = 1.0
			H continuum	2.1(-18)	10.2	f = 1.0
10	11.2	13.6	H_2 Werner and photoionization	1.26(-17)	0	f = 0.4
			C continuum	1.4(-17)	0	f = 1.0
			Si continuum	2.38(-18)	0.166	f = 1.0
			H continuum	2.1(-18)	10.2	f = 1.0

TABLE 5 (cont'd)

Band No.	Frequency, eV Lower	Upper	System	σ_0 (cm^2)	B (eV)	Remarks
11	13.6	19.0	CO photo ionization	1.0(-17)	0	f = 1.0
			C continuum	1.4(-17)	0.178	f = 1.0
			Si continuum	2.64(-18)	0.310	f = 1.0
			H continuum	4.85(-18)	0	f = 1.0
12	19.0	24.4	CO photo-ionization	1.7(-17)	0	f = 1.0
			C continuum	1.4(-17)	0.178	f = 1.0
			Si continuum	2.98(-18)	0.487	f = 1.0
			H continuum	2.0(-18)	0	f = 1.0
			O continuum	3.5(-18)	0	f = 1.0
			C+ continuum	4.2(-13)	23.6	f = 1.0

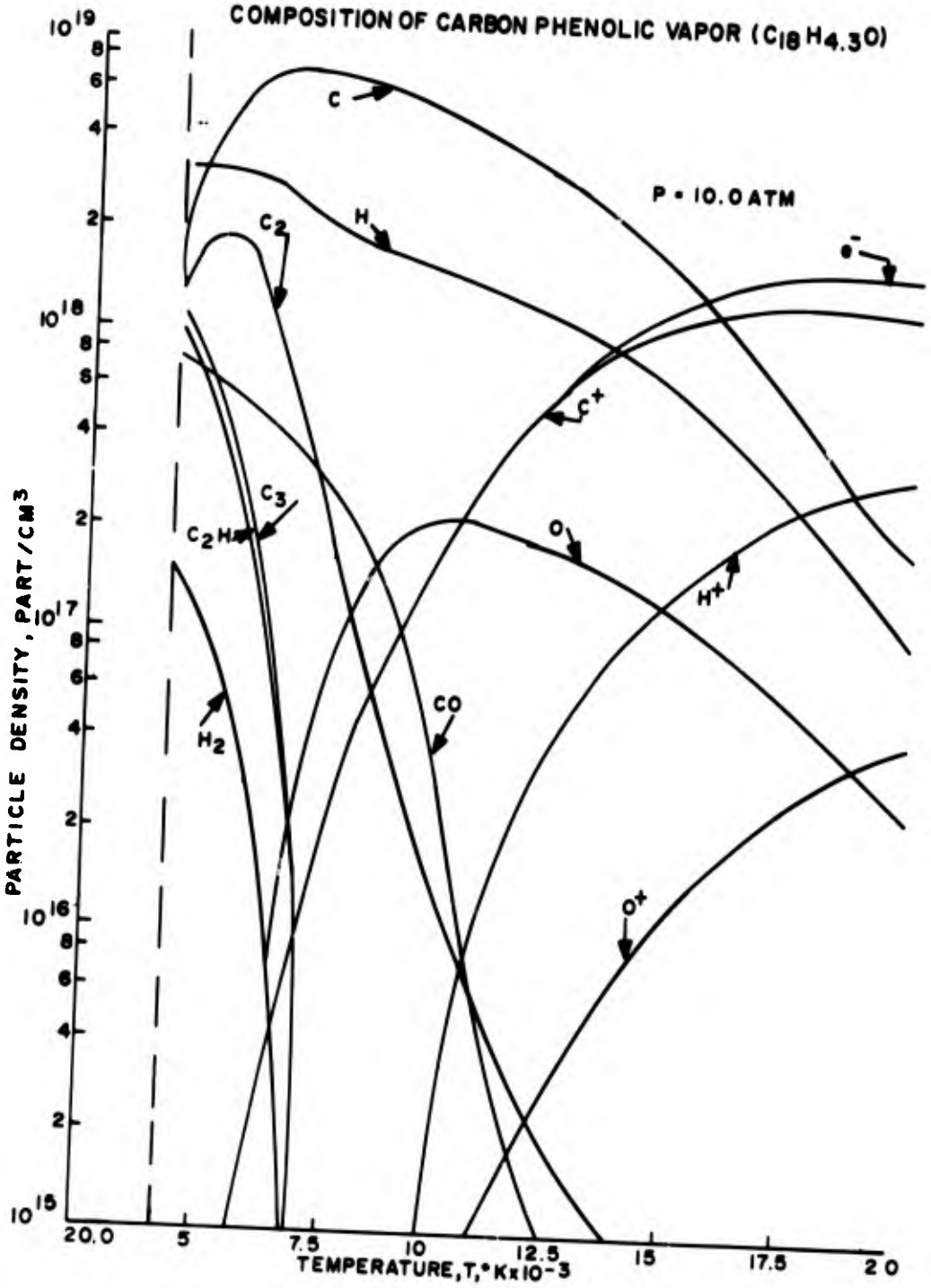

Fig 1 Particle density vs temperature for carbon phenolic at 10.0 atmospheres

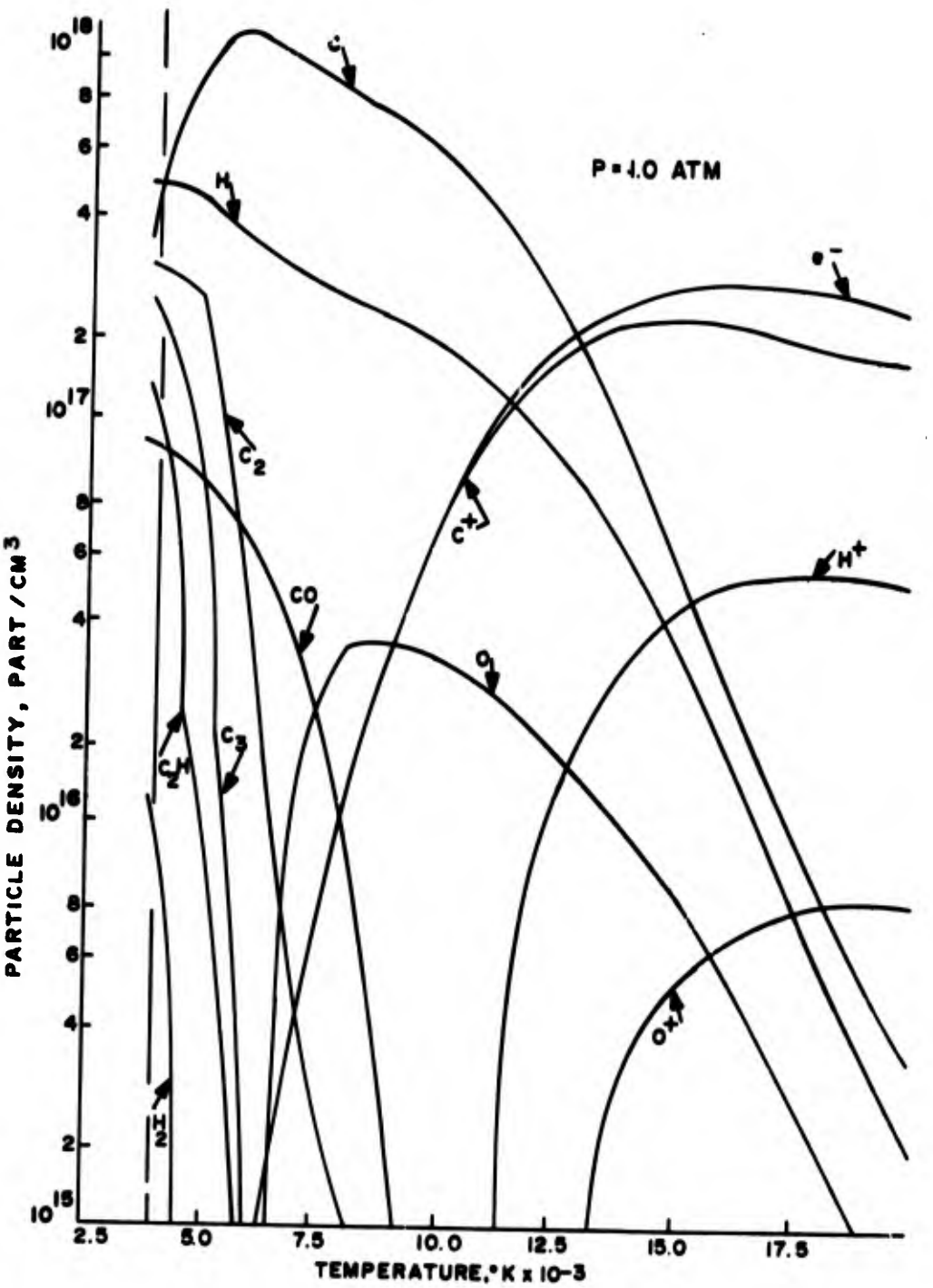

Fig 2 Particle density vs temperature for carbon phenolic at 1.0 atmosphere

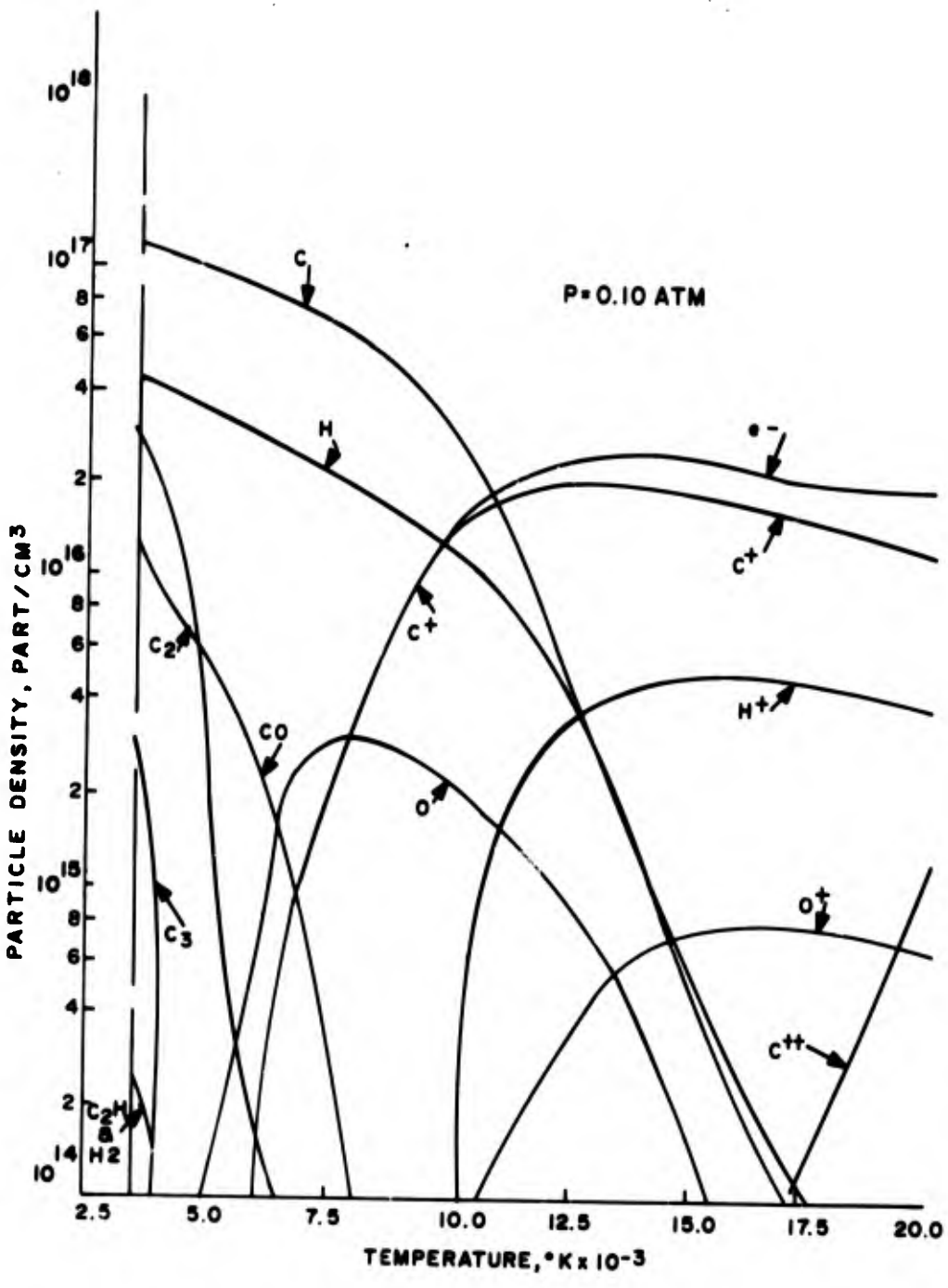

Fig 3 Particle density vs temperature for carbon phenolic at 0.10 atmosphere

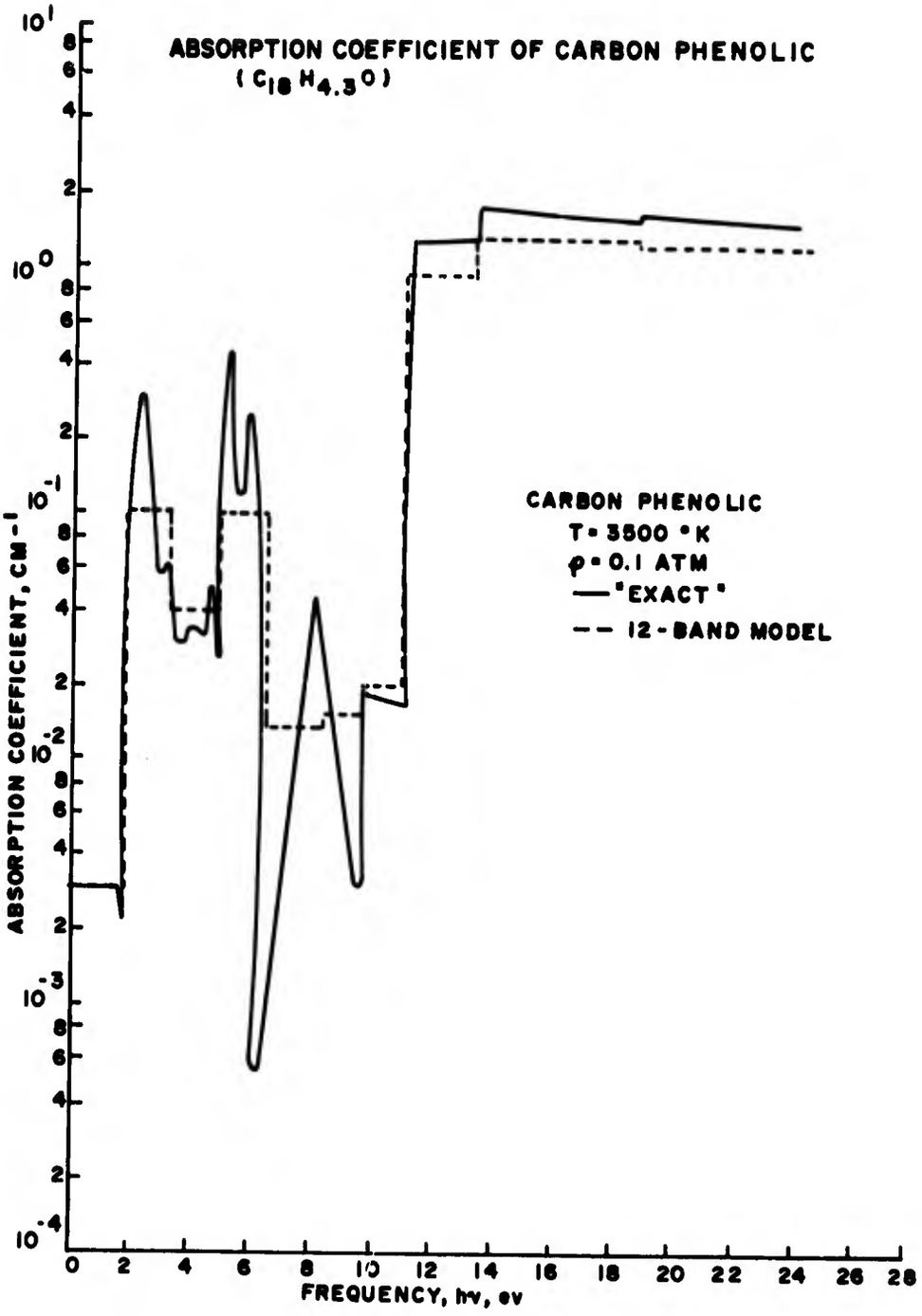

Fig 4 Comparison of "exact" and 12-band model uncorrected absorption coefficients at 3500°K and 0.1 atmosphere

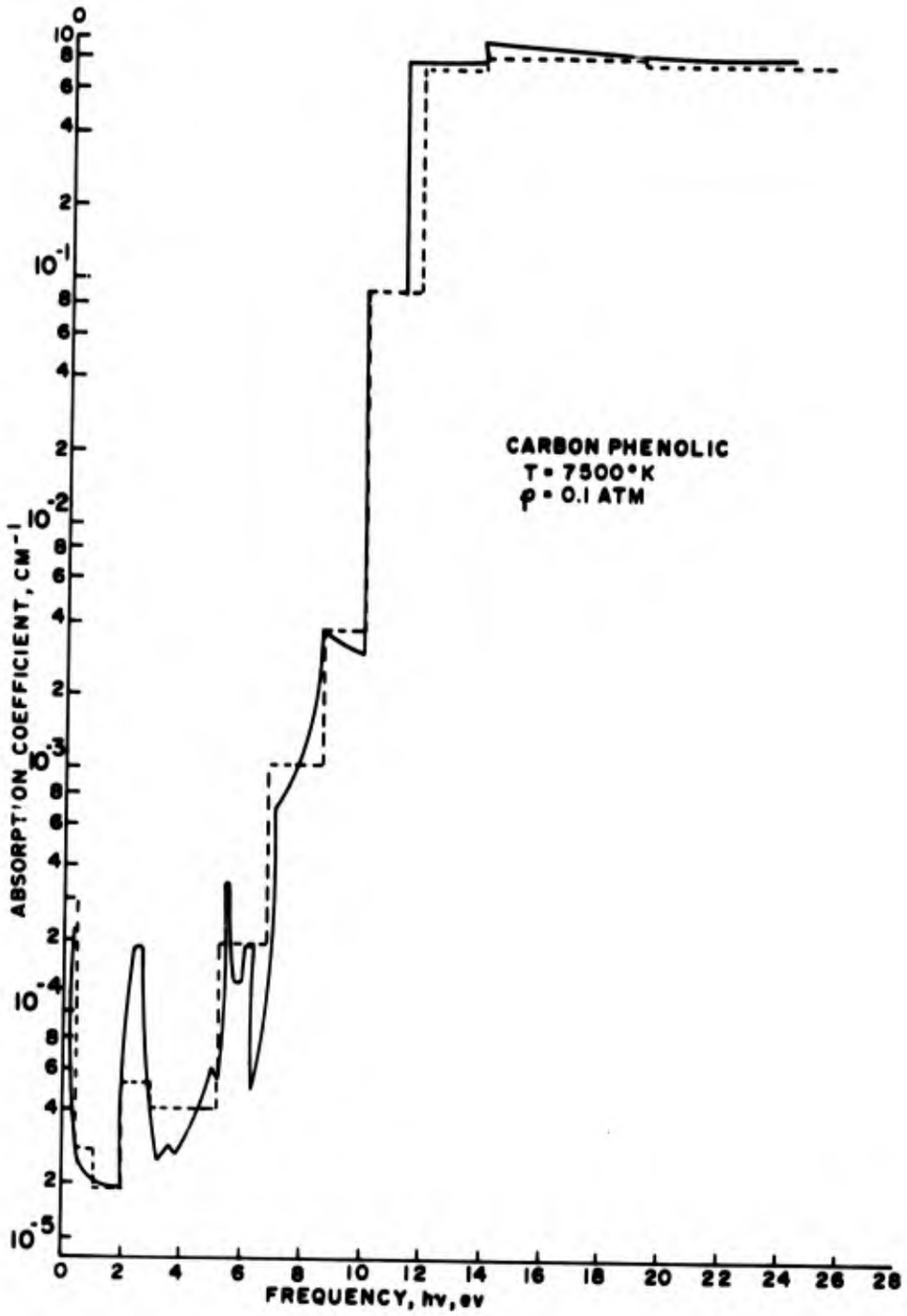

Fig 5 Comparison of "exact" and 12-band model uncorrected absorption coefficients at 7500°K and 0.1 atmosphere

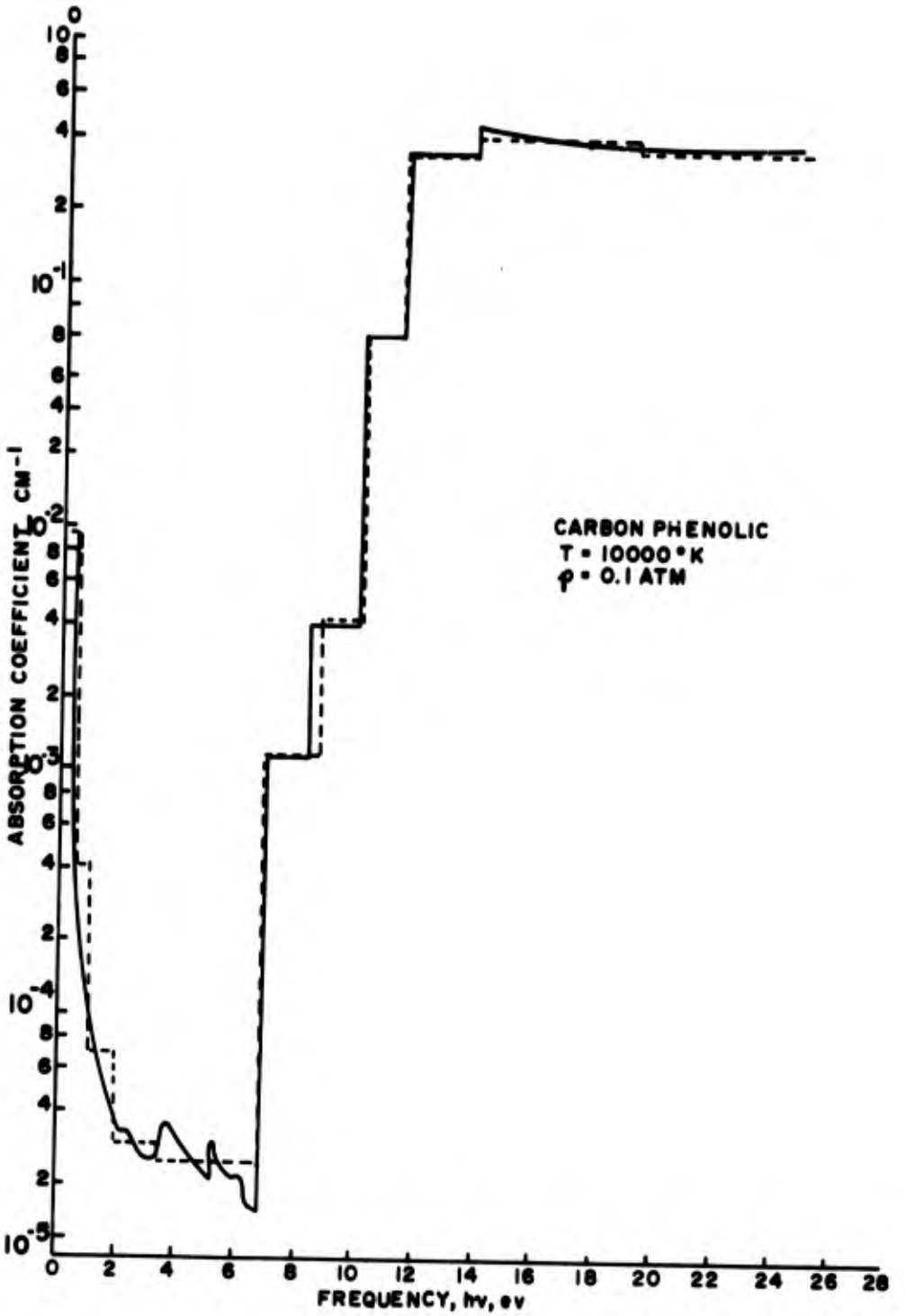

Fig 6 Comparison of "exact" and 12-band model uncorrected absorption coefficients at 10000°K and 0.1 atmosphere

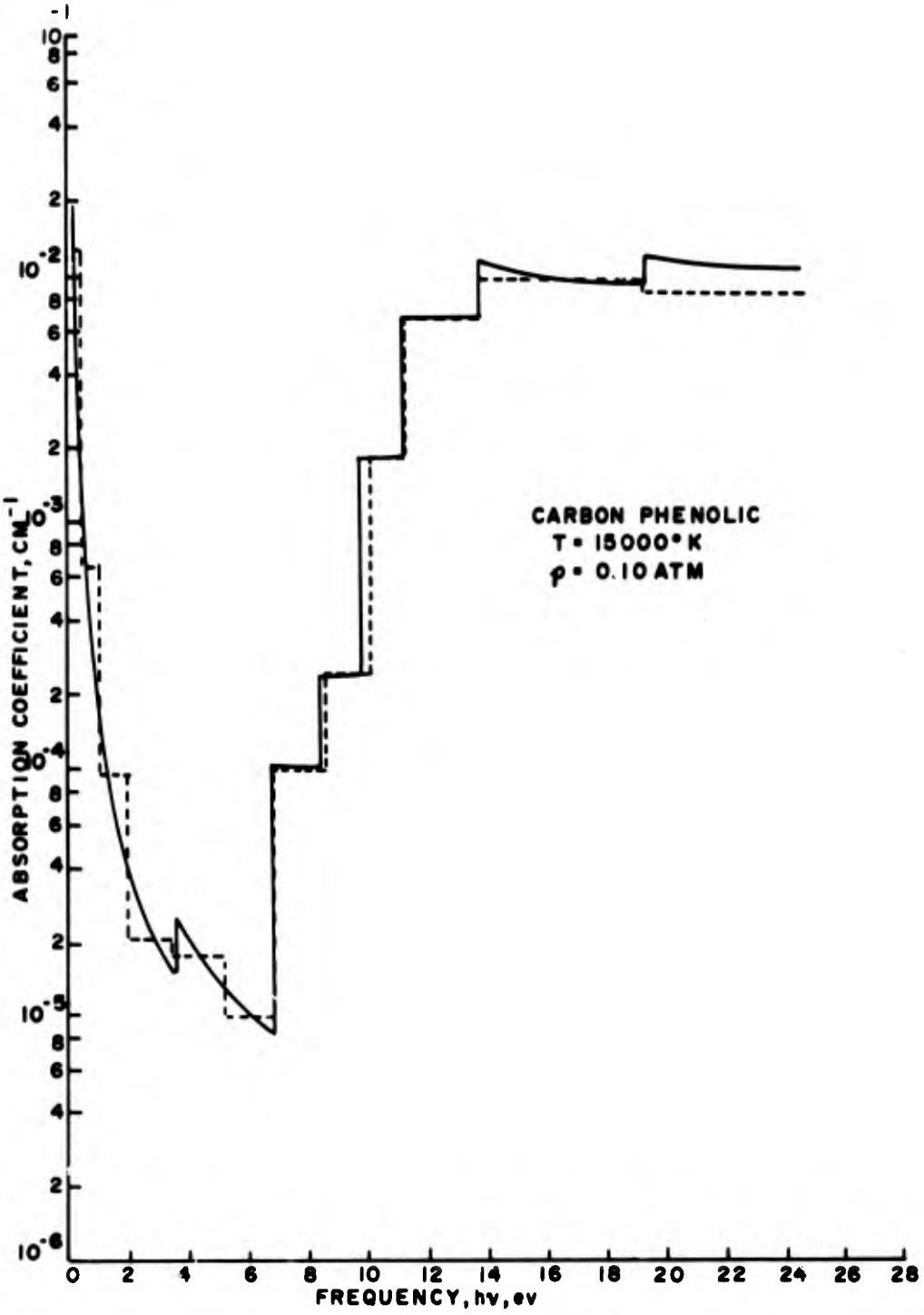

Fig 7 Comparison of "exact" and 12-band model uncorrected absorption coefficients at 15000°K and 0.1 atmosphere

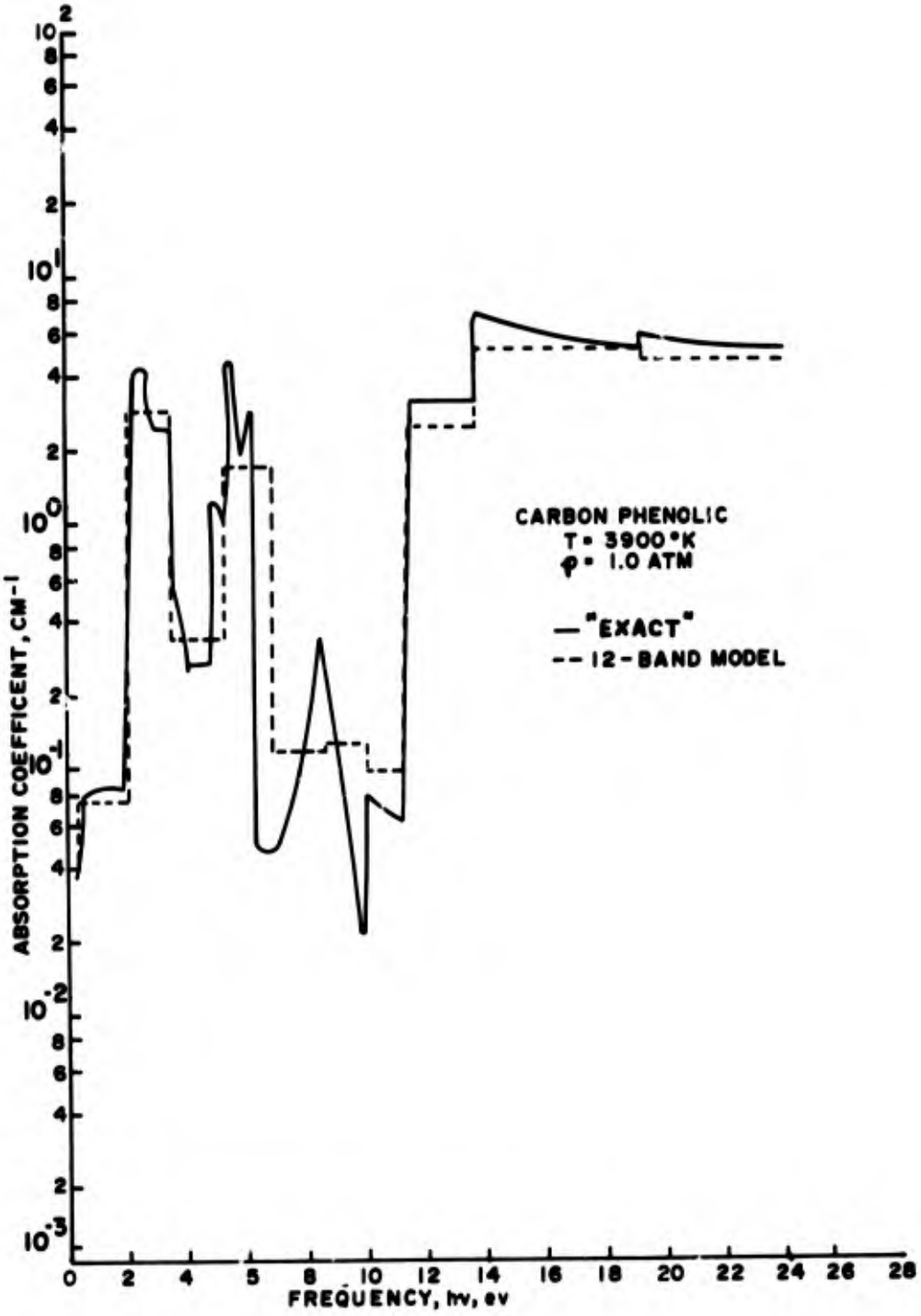

Fig 8 Comparison of "exact" and 12-band model uncorrected absorption coefficients at 3900°K and 0.1 atmosphere

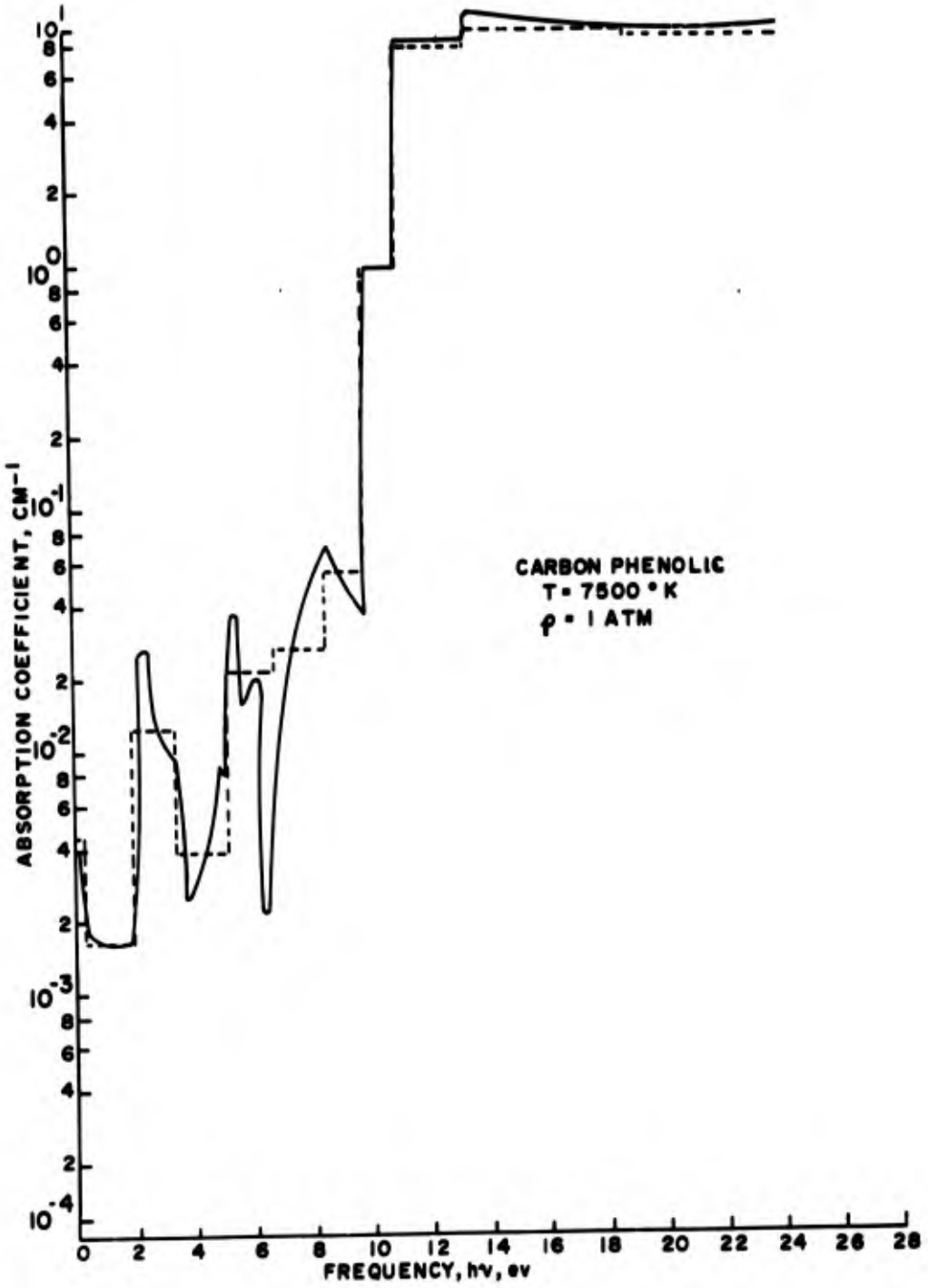

Fig 9 Comparison of "exact" and 12-band model uncorrected absorption coefficients at 7500°K and 1.0 atmosphere

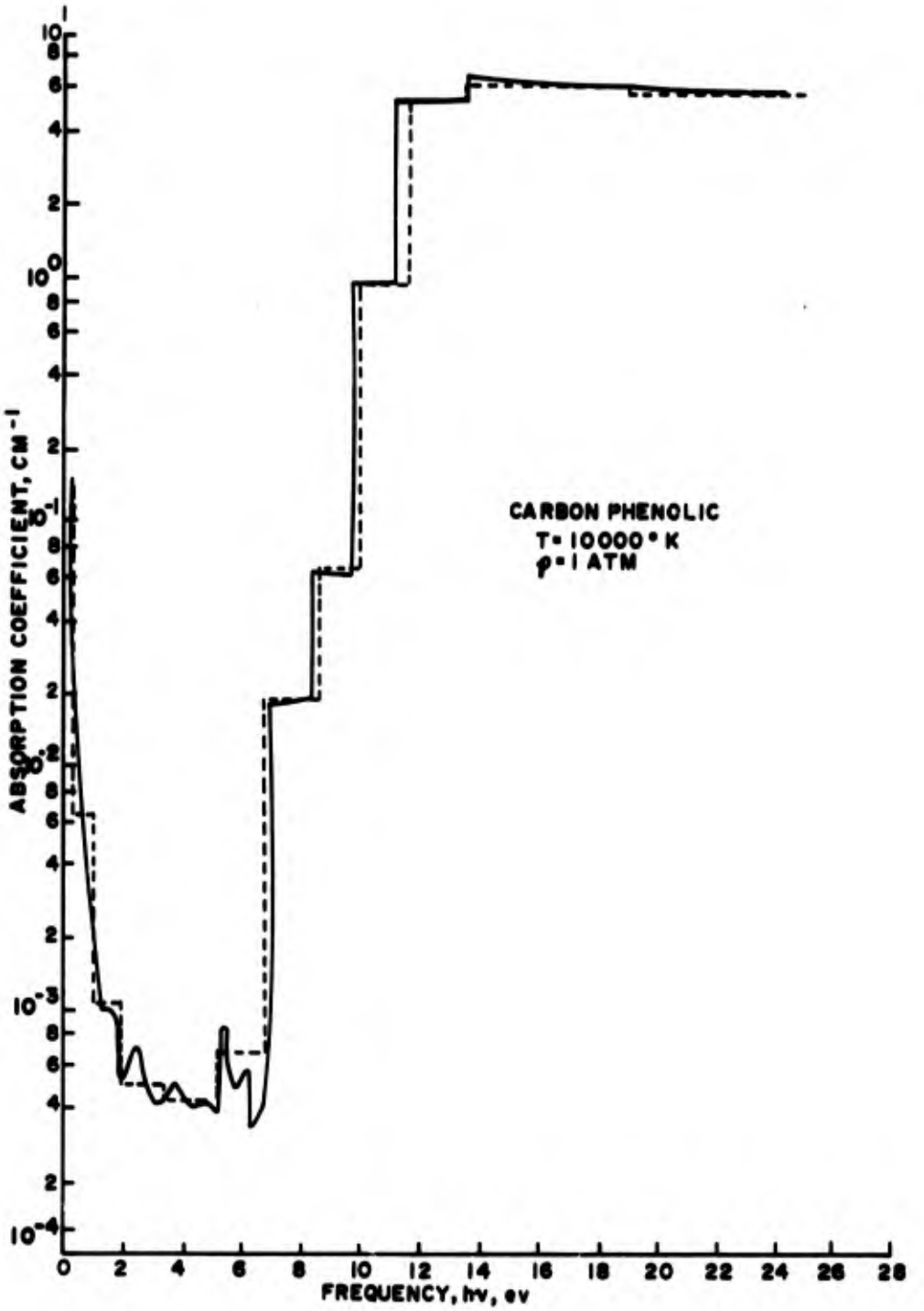

Fig 10 Comparison of "exact" and 12-band model uncorrected absorption coefficients at 10000°K and 1.0 atmosphere

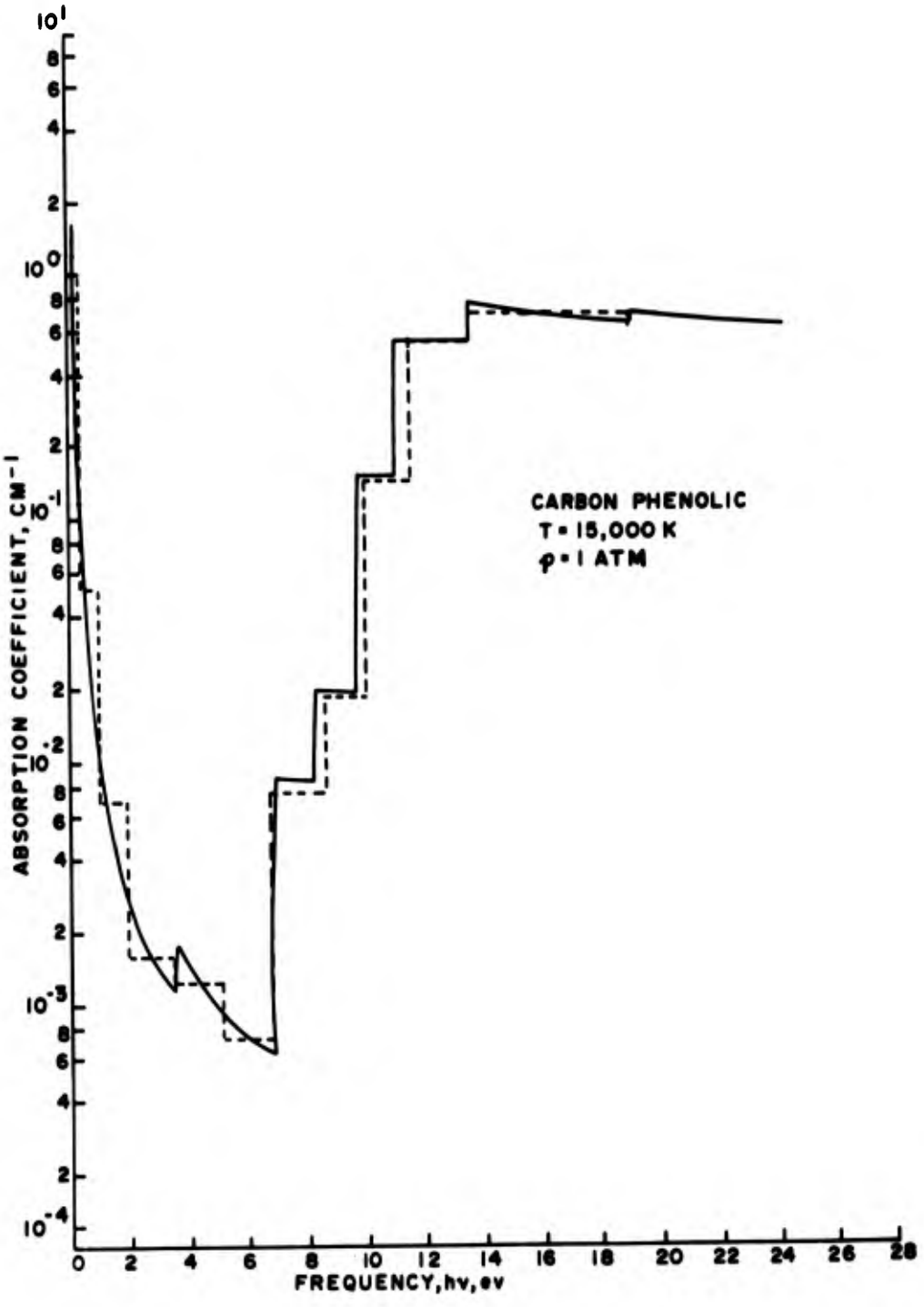

Fig 11 Comparison of "exact" and 12-band model uncorrected absorption coefficients at 15000°K and 1.0 atmosphere

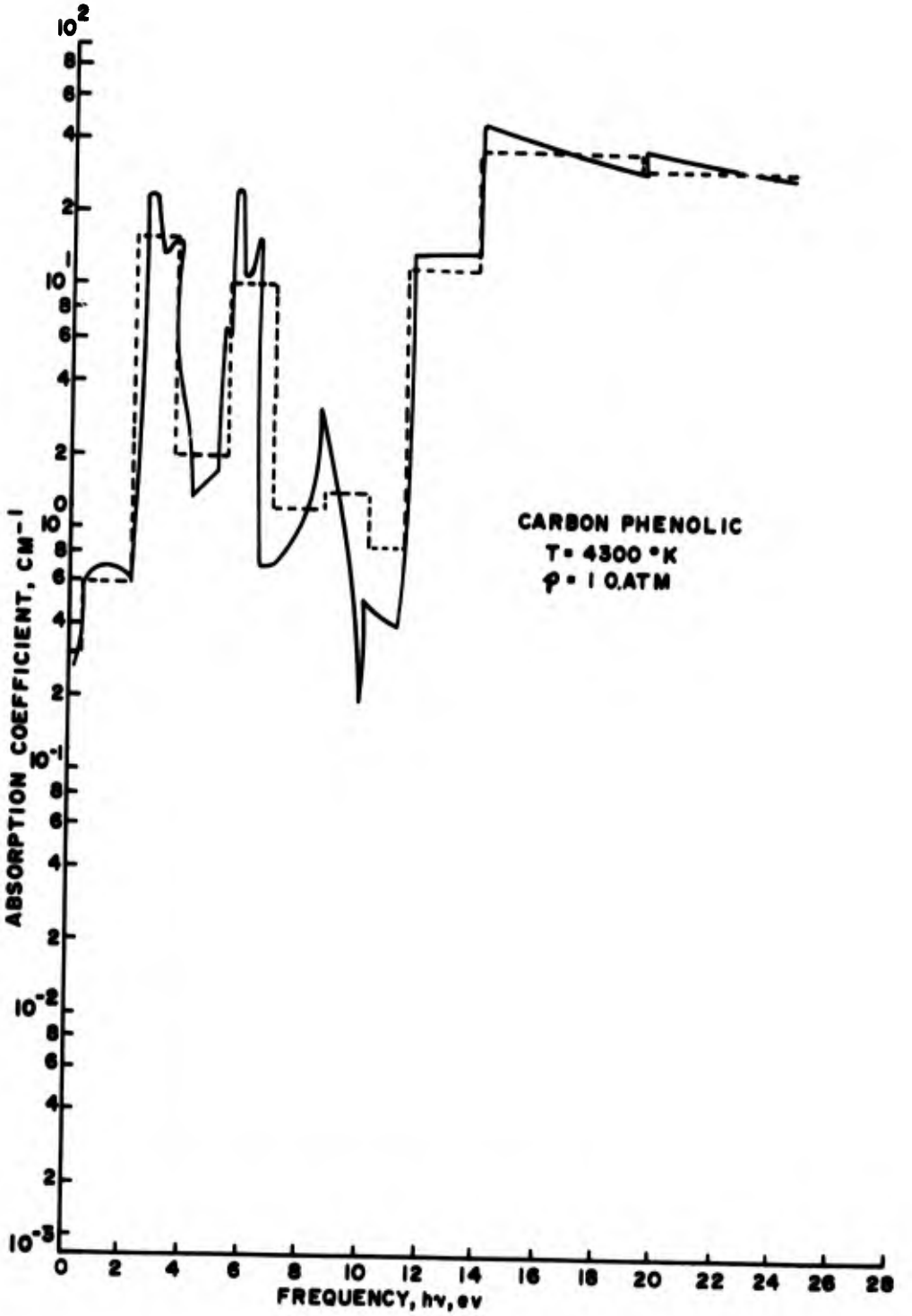

Fig 12 Comparison of "exact" and 12-band model uncorrected absorption coefficients at 4300°K and 10.0 atmospheres

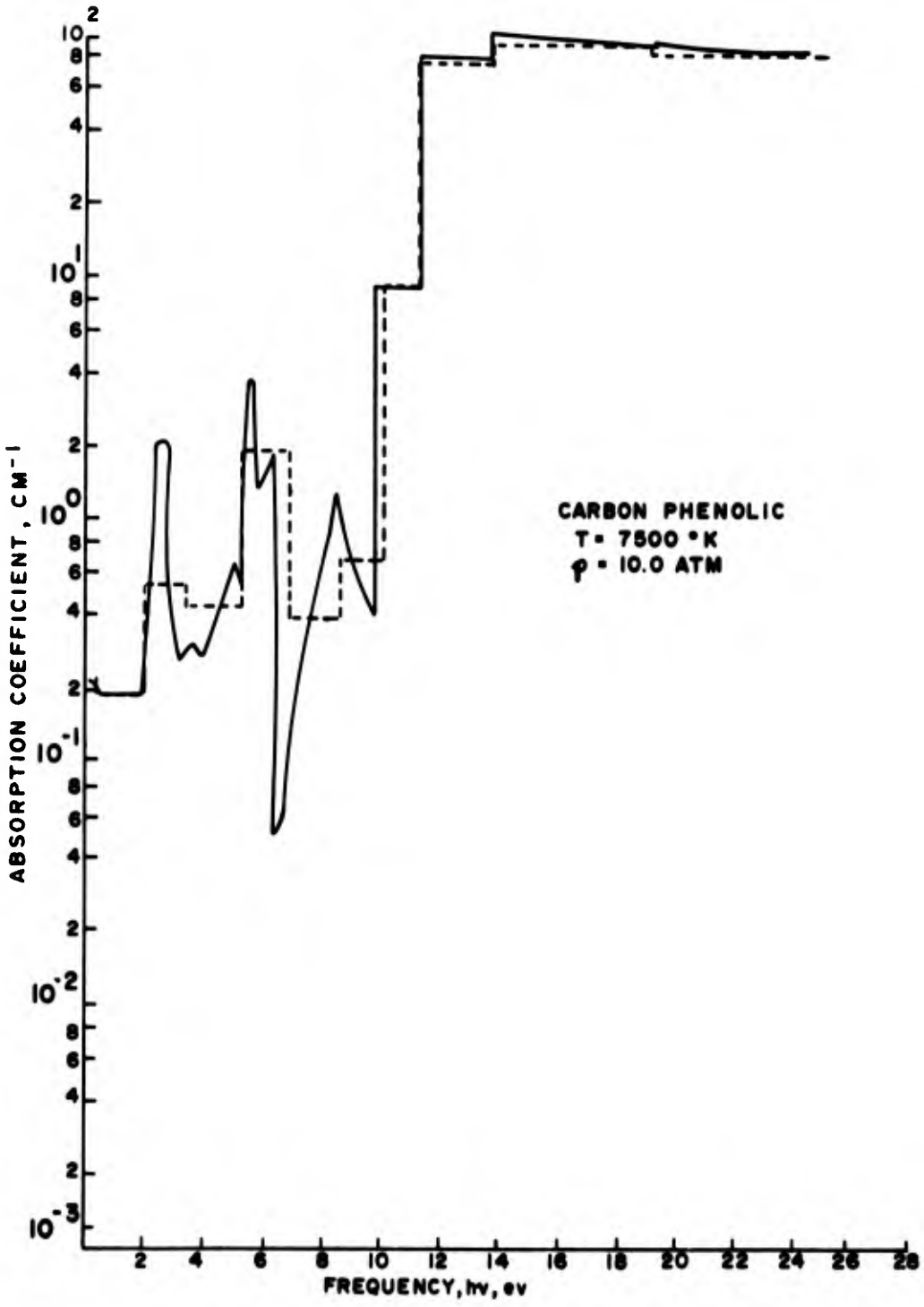

Fig 13 Compariosn of "exact" and 12-band model uncorrected absorption coefficients at 7500°K and 10.0 atmospheres

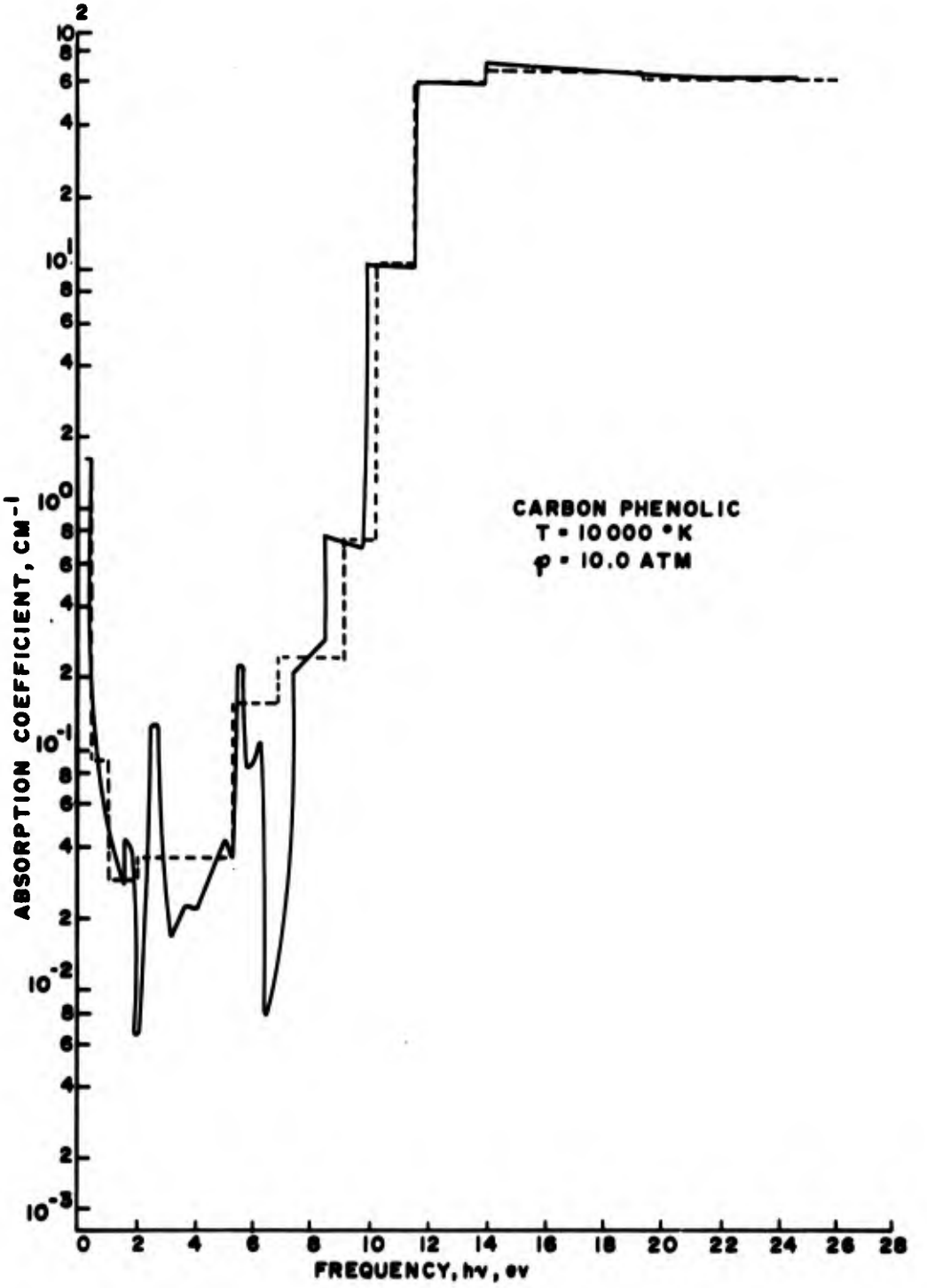

Fig 14 Comparison of "exact" and 12-band model uncorrected absorption coefficients at 10000°K and 10.0 atmospheres

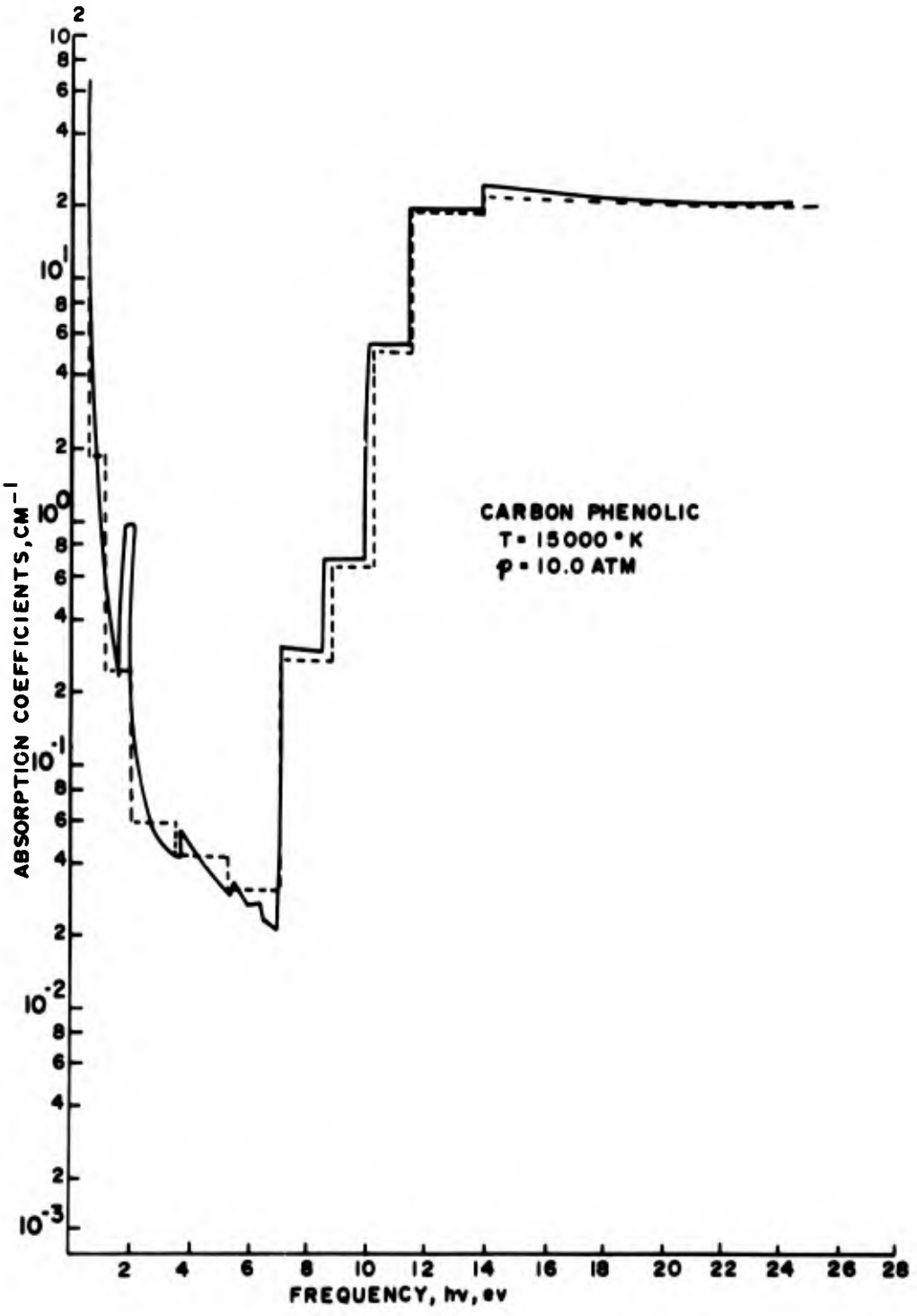

Fig 15 Comparison of "exact" and 12-band model uncorrected absorption coefficients at 15000°K and 10.0 atmospheres

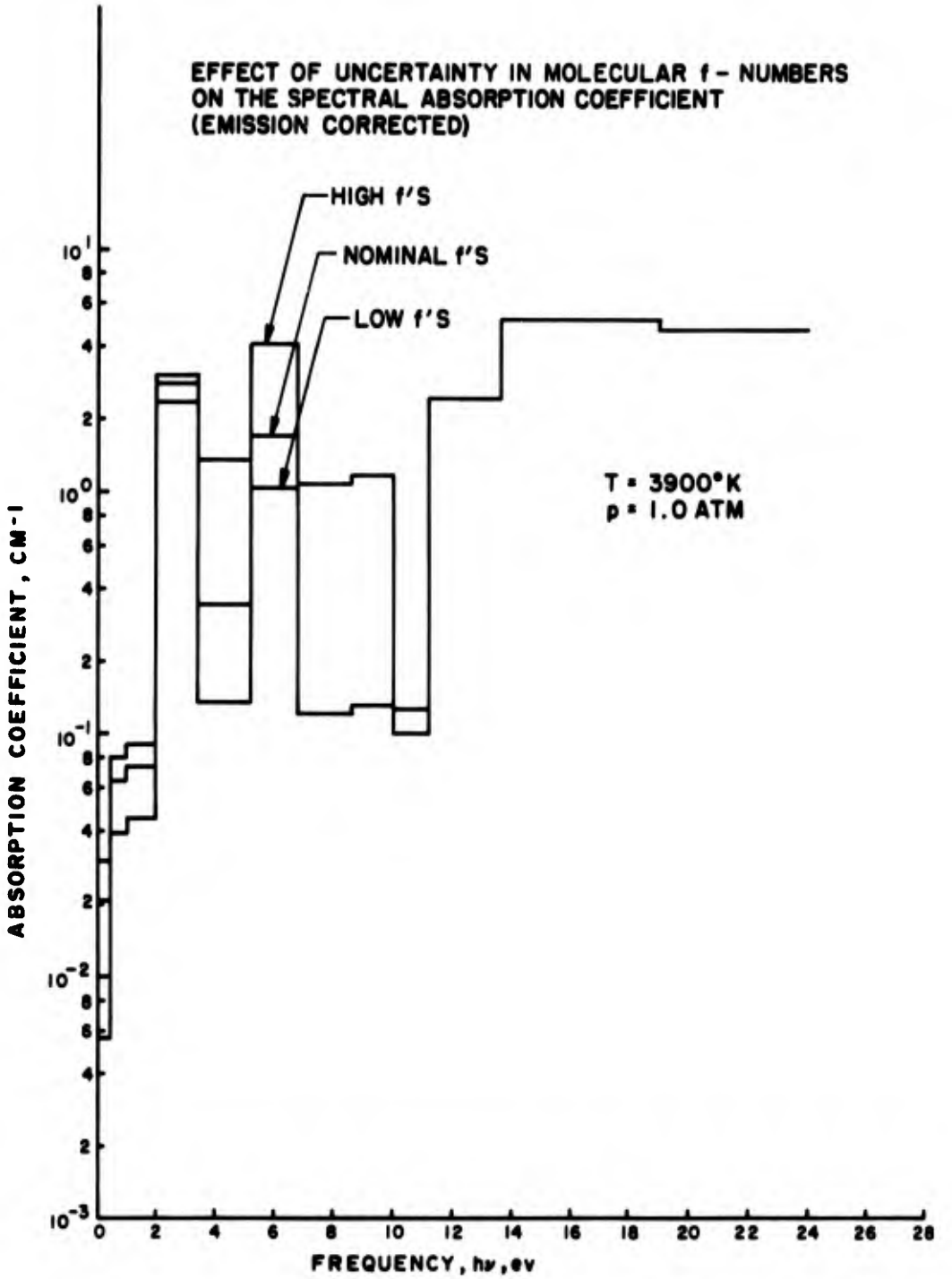

Fig 16 Effect of uncertainty of molecular f-number on emission corrected absorption coefficient at 3900^{O}K and 1.0 atmosphere

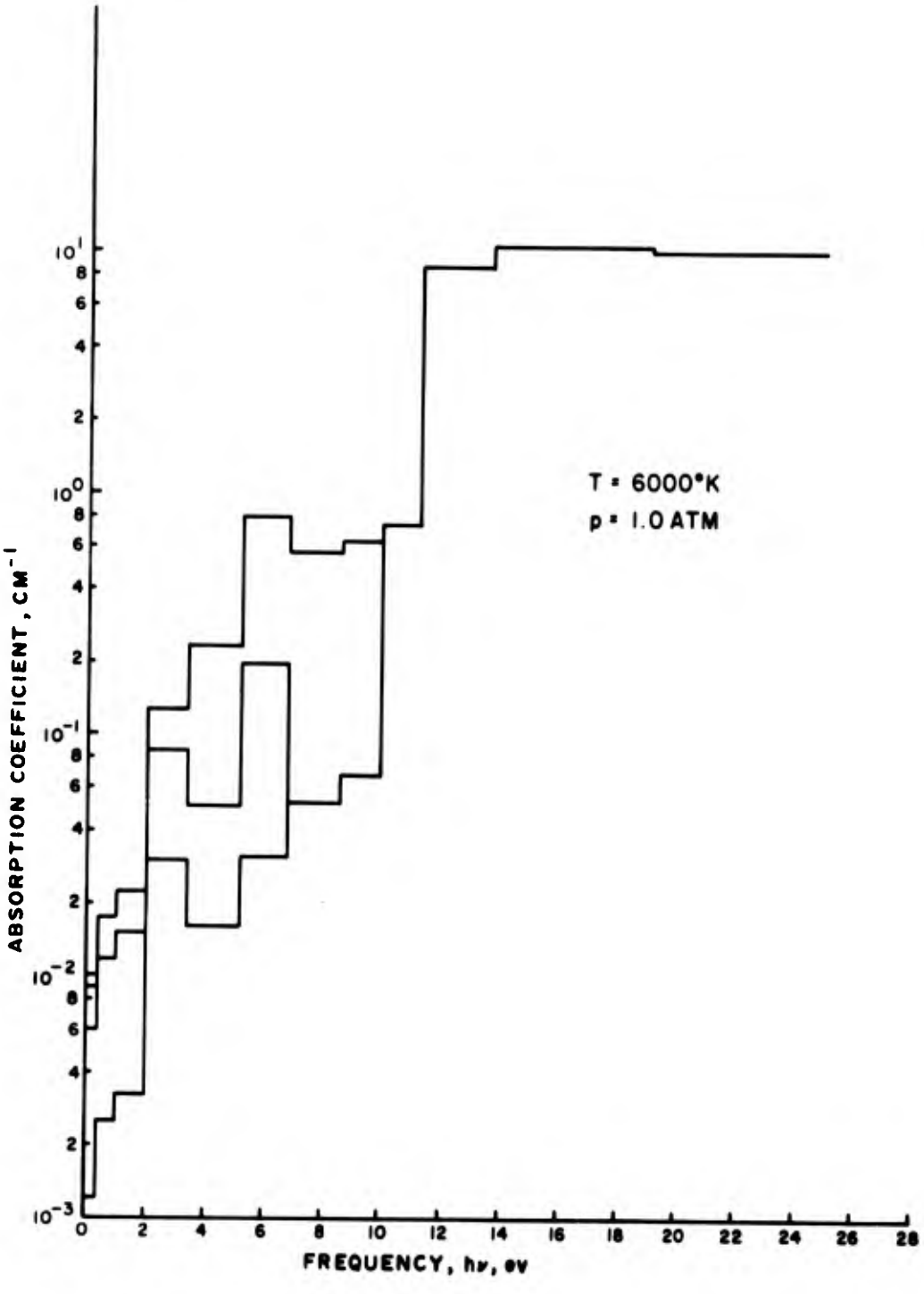

Fig 17 Effect of uncertainty of molecular f-number on emission corrected absorption coefficient at 6000^{o}K and 1.0 atmosphere

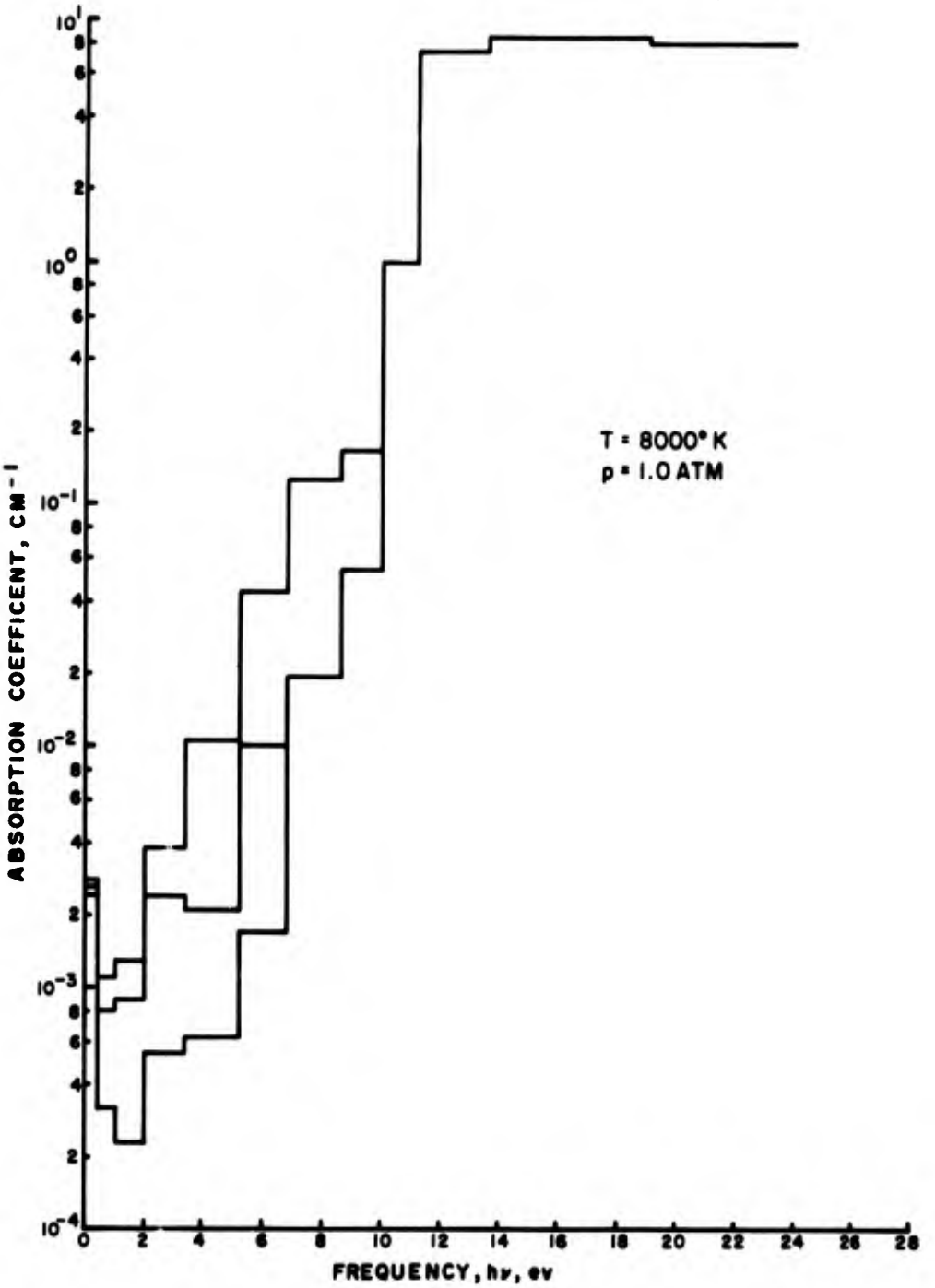

Fig 18 Effect of uncertainty of molecular f-number on emission corrected absorption coefficient at 8000°K and 1.0 atmosphere

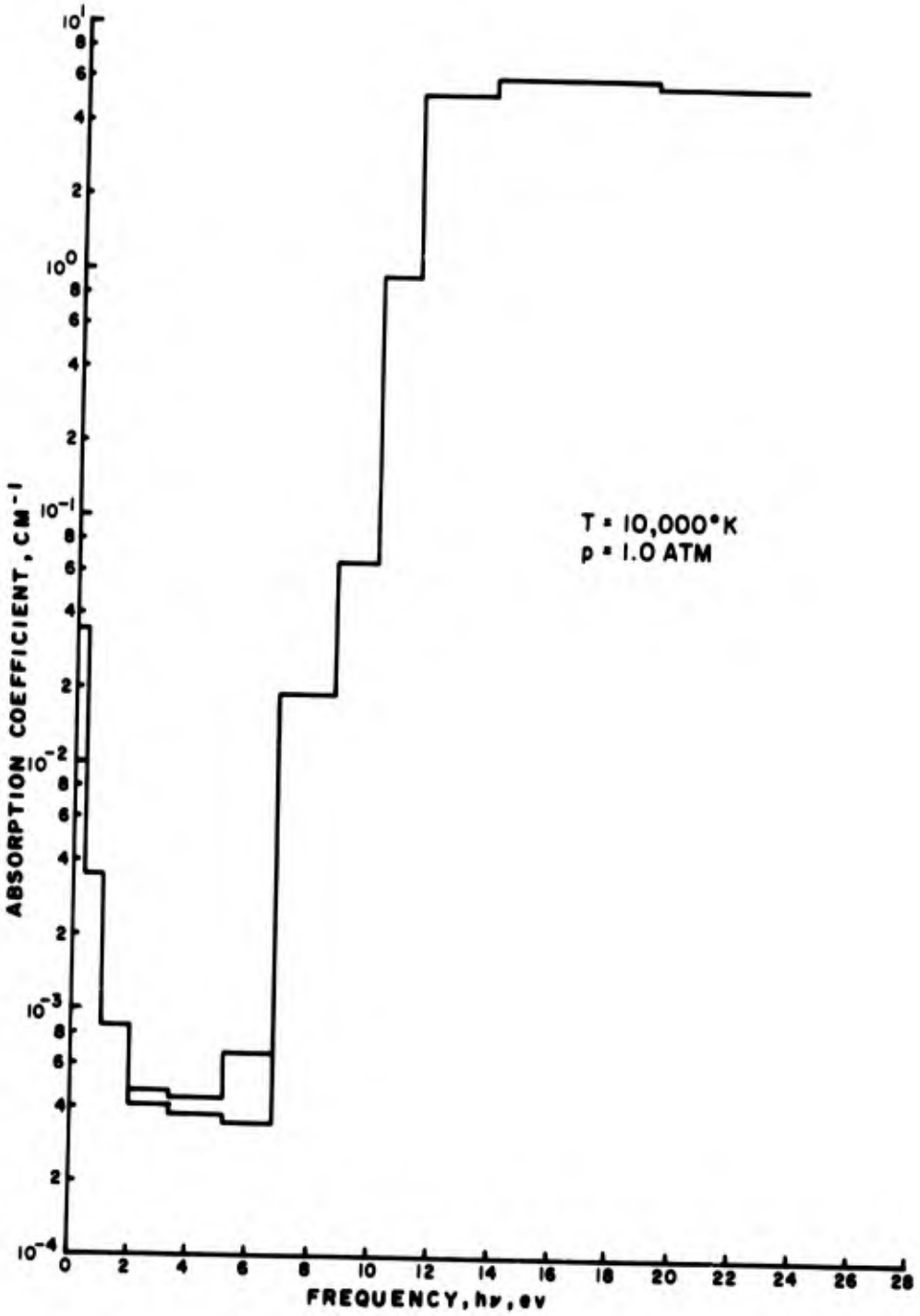

Fig 19 Effect of uncertainty of molecular f-number on emission corrected absorption coefficient at 10000^{O}K and 1.0 atmosphere

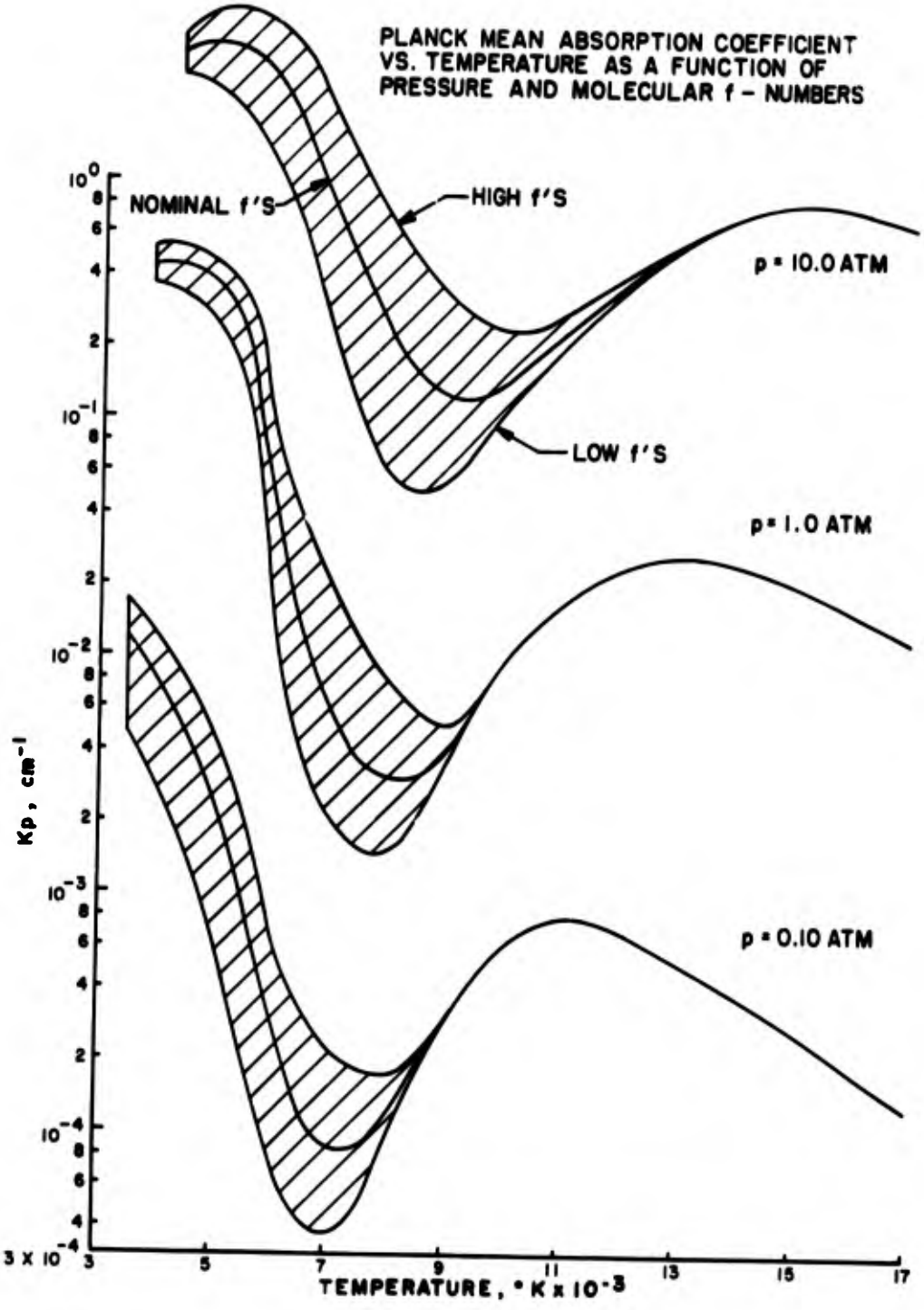

Fig 20 Planck mean absorption coefficient vs temperature as a function of pressure and molecular f-number

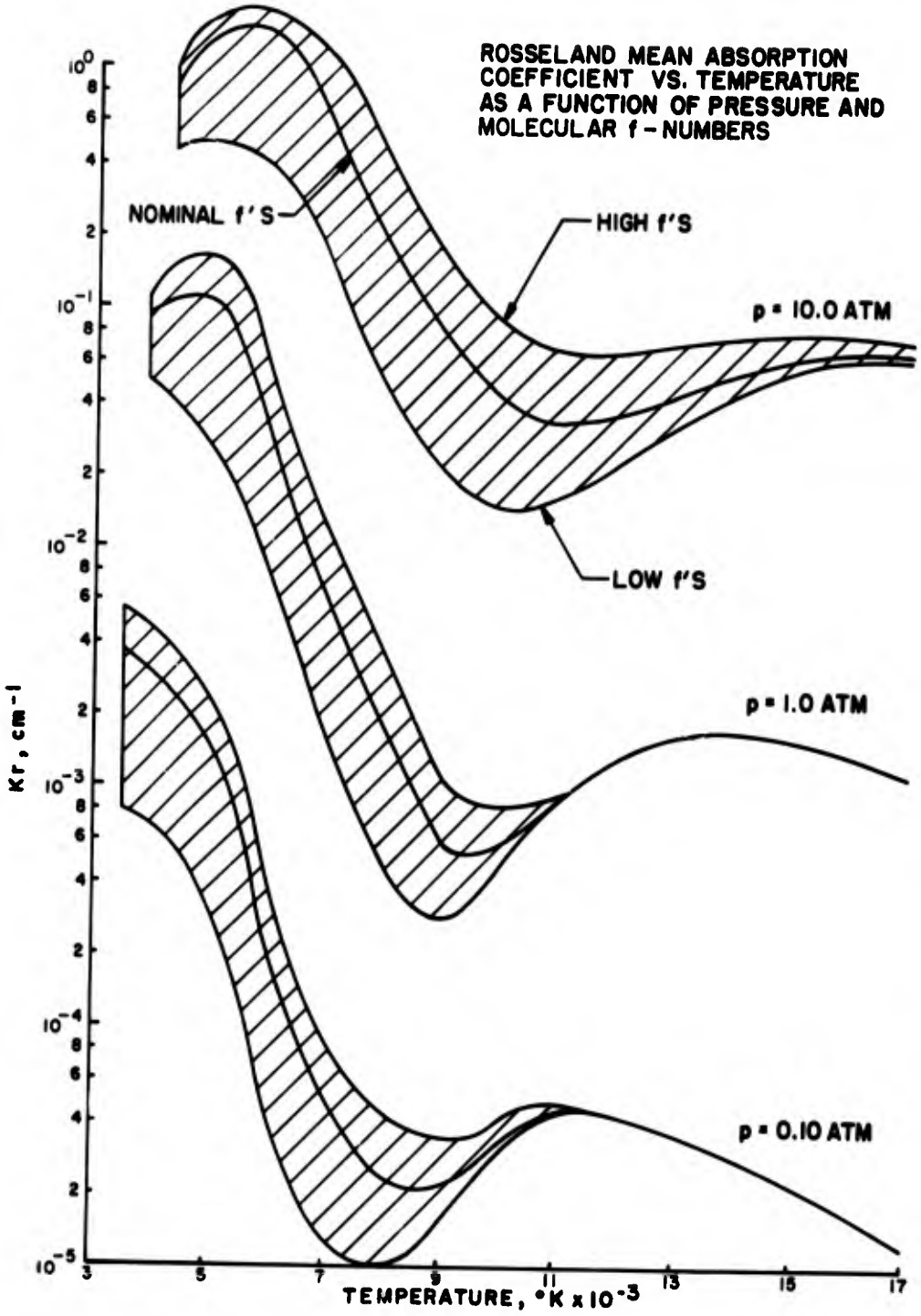

Fig 21 Rosseland mean absorption coefficient vs temperature as a function of pressure and molecular f-number

APPENDIX A

Description of program ABSORB

Input Quantities

NT	Number of temperatures in input tables
NS	Number of species in input tables
NYY	Number of temperatures at which calculations are to be made
NNN	Currently not used
P	Pressure in atmospheres for calculations
TEE	Temperature array at which calculations are to be made, ^{o}K
TT	Input temperature array for number density data, ^{o}K
ST^{1}	Number density array, part/cm^{3}
FRS	Ratio of molecular f-number to nominal C_2: Swan
FRH	Ratio of molecular f-number to nominal C_2: Fox-Herzberg
FRD	Ratio of molecular f-number to nominal C_2: Deslandres-d'Azambuja
FRF	Ratio of molecular f-number to nominal C_2: Mulliken
FR4P	Ratio of molecular f-number to nominal CO: 4+
FRA	Ratio of molecular f-number to nominal CO: Asundi

FRPH	Ratio of molecular f-number to nominal CO: photo
FRN	Ratio of molecular f-number to nominal not used at present
FRCNV	Ratio of molecular f-number to nominal C_2H: violet (CN)
FRCNR	Ratio of molecular f-number to nominal C_2H: red (CN)
FR3L	Ratio of molecular f-number to nominal C_3: λ 4056
FR3V	Ratio of molecular f-number to nominal C_3: violet
FRAX	Ratio of molecular f-number to nominal SiO: A-X

[1] Species data must be given in the order: H, C, C^+, N, N^+, O, O^+, e^-, N^-, O^-, O_2, N_2, CO, H_2, C_2, CN, C_2H, C_3, H^+, C_2^-, Si, Si^+, SiO

Output Quantities

ANN	Number densities at required temperature
ALFA1	Uncorrected absorption coefficient in 1st band
ALFA(1,I)	Corrected absorption coefficient in 1st band
ALFA2	Uncorrected absorption coefficient in 2nd band
ALFA(2,I)	Corrected absorption coefficient in 2nd band
ALFA3	Uncorrected absorption coefficient in 3rd band
ALFA(3,I)	Corrected absorption coefficient in 3rd band

ALFA4	Uncorrected absorption coefficient in 4th band
ALFA(4, I)	Corrected absorption coefficient in 4th band
ALFA5	Uncorrected absorption coefficient in 5th band
ALFA(5, I)	Corrected absorption coefficient in 5th band
ALFA6	Uncorrected absorption coefficient in 6th band
ALFA(6, I)	Corrected absorption coefficient in 6th band
ALFA7	Uncorrected absorption coefficient in 7th band
ALFA(7, I)	Corrected absorption coefficient in 7th band
ALFA8	Uncorrected absorption coefficient in 8th band
ALFA(8, I)	Corrected absorption coefficient in 8th band
ALFA9	Uncorrected absorption coefficient in 9th band
ALFA(9, I)	Corrected absorption coefficient in 9th band
ALFA10	Uncorrected absorption coefficient in 10th band
ALFA(10, I)	Corrected absorption coefficient in 10th band
ALFA11	Uncorrected absorption coefficient in 11th band
ALFA(11, I)	Corrected absorption coefficient in 11th band
ALFA12	Uncorrected absorption coefficient in 12th band
ALFA(12, I)	Corrected absorption coefficient in 12th band
ALFAB1	IR absorption coefficient in 2-band model
ALFAB2	UV absorption coefficient in 2-band model
PLKMN	Planck mean absorption coefficient
ROSSL	Rosseland mean absorption coefficient

```
CARD
NUMBER
     1        MLOSINS AMSC88
     2        C
     3        C      AMSCRPTION COEFFICIENTS OF ABLATORS
     4        C
     5              COMMON/TABLES/ ST(25,100),TT(100),TEE(100),ANN(25,100),
     6             1 ALFA(12,100),ALFAB1(100),ALFAB2(100),G(100),F(100),RHO(100)
     7             2,RCSSL(100),PLKMA(100)
     8        C
     9              NREAD=5
    10              NWRITE=6
    11        C
    12            1 READ(NREAD,101) AT,AS,NYY,NAN,P
    13          101 FORMAT(4I5,6F10.4)
    14        C
    15              WRITE(NWRITE,140)
    16          140 FORMAT(///,20X,43HTOTAL ABSORPTION COEFFICIENTS-12 BAND MODEL,///)
    17        C
    18              WRITE(NWRITE,300) P
    19          300 FORMAT(//,10X,11HPRESSURE = ,F10.4,3X,4HATM.,//)
    20        C
    21              READ(NREAD,100) (TEE(I),I=1,NYY)
    22              READ(NREAD,100) (TT(M),M=1,NT)
    23          100 FORMAT(5G12.5)
    24          110 FORMAT(5(12X,6G12.5/))
    25              DO 4 M=1,NT
    26              READ(NREAD,100) ( ST(J,M),J=1,NS)
    27            4 CONTINUE
    28              READ(NREAD,100) FRS,FRFH,FRC,FRF,FRM,FR4P
    29              READ(NREAD,100) FRA,FRFH,FRN,FRCNV,FRCNR
    30              READ(NREAD,100) FR3L,FR3V,FRAX
    31        C
    32              WRITE(NWRITE,150)
    33          150 FORMAT(//,05X,'F-NUMBER RATIO REFERENCED TO WEISNER OR LMSC',/)
    34        C
    35              WRITE(NWRITE,170)
    36          170 FORMAT(/,6X,3HFRS,9X,4HFRFH,8X,3HFRC,9X,3HFRF,9X,3HFRM,9X,4HFR4P,/
    37             1,4X,3HFRA,9X,4HFRFH,8X,3HFRN,8X,5HFRCNV,7X,5HFRCNR,/,4X,4HFR3L,8X,
    38             2  4HFR3V,9X,4HFRAX,/)
    39        C
    40              WRITE(NWRITE,110) FRS,FRFH,FRC,FRF,FRM,FR4P
    41              WRITE(NWRITE,110) FRA,FRFH,FRN,FRCNV,FRCNR
    42              WRITE(NWRITE,110) FR3L,FR3V,FRAX
    43              DO 5 I=1,NYY
    44              CALL EMPP (AT,AS,NYY,AERR,I)
    45            5 CONTINUE
    46        C
    47              DO 3 I=1,NYY
    48        C
    49              WRITE(NWRITE,130)
    50          130 FORMAT(1H1,20X,'NEW TEMPERATURE CALCULATION',/ )
    51        C
    52              WRITE(NWRITE,400) TEE(I)
    53          400 FORMAT( /,10X,14HTEMPERATURE = ,G12.5,2X,6HDEG. K,/ )
    54        C
    55              WRITE(NWRITE,200)
    56          200 FORMAT( /,15X,42HSPECIES NUMBER DENSITIES   PARTICLES/CM**3,/ ,
    57             1  7X,1HH,11X,1HC,11X,2HC+,10X,1HH,11X,2HN+,10X,1HO,/,
    58             2  7X,2HO+,10X,2HE-,10X,2HA-,10X,2HO-,10X,2HO2,10X,2HN2,/,
```

```
CARD
NUMBER
   58      3 7X,2HCO,10X,2HH2,10X,2HC2,10X,2HCH,10X,3HC2H,5X,3HC3,/,
   59      4 7X,2HH ,10X,3HC2-,9X,3HSI,10X,3HSI+,9X,3HSI0,//)
   60
   61      WRITE(NWRITE,110) (XAA(J,I),J=1,NS)
   62
   63      WRITE(NWRITE,410)
   64  410 FORMAT(///,10X,'PHOTO NO.',5X,'FREQUENCY RANGE (EV)',14X,'SHIELD
   65     1ING COEFFICIENT (1/CM)',/ 57X,'UNCORRECTED',2X,'CORRECTED',/)
   66
   67      TK=TES(I)
   68      T=TES(I)/11606.
   69
   70  C
   71  C     BAND  1 CALCULATIONS, FREQUENCY =  0.10 TO  0.40 ELECTRON VOLTS
   72  C
   73      FAC1=(1.55E-16*EXP(-1.2/T))
   74      FAC2=0.0
   75      FAC3=(7.04E-17*EXP(-7.18/T))
   76      FAC4=4.0E-18
   77      FAC14=1.33E-13*EXP(-11.2/T)
   78      FAC9=1.0E-14*T*EXP(-13.2/T)
   79      FAC19=FAC9
   80      AL11  =FAC1*XAA(15,I)*0.029
   81      AL21  =0.0
   82      AL31  =FAC3*XAA(21,I)
   83      AL41  =FAC4*XAA(17,I)*0.008
   84      AL91  =FAC9*XAA(1  ,I)
   85      AL141  =FAC14*XAA(2  ,I)
   86      AL191  =FAC19*XAA(5  ,I)
   87      ALFAE=0.0
   88      ALFA1  =AL11*FRS+AL21+AL31+AL41*FRCNR+AL141+ALFAE+AL91+AL191
   89  C
   90  C     CORRECTION FOR INDUCED EMISSION
   91  C
   92      ALF1(1,I)=(1.+3.333*T*(EXP(-0.4/T)-EXP(-0.1/T)))*ALFA1
   93  C
   94      WRITE(NWRITE,201) ALFA1,ALFA(1,I)
   95  201 FORMAT(/,14X,2H01,10X,14H00.10 TO 00.40,18X,2G12.5,/)
   96  C
   97  C     BAND  2 CALCULATIONS, FREQUENCY =  0.40 TO  1.00 ELECTRON VOLTS
   98  C
   99      FAC1=(1.86E-16*EXP(-1.2/T))
  100      FAC2=0.0
  101      FAC3=(7.04E-17*EXP(-7.18/T))
  102      FAC4=4.0E-17
  103      FAC14=8.65E-15*EXP(-11.5/T)
  104      FAC9=4.0E-16*T*EXP(-12.8/T)
  105      FAC19=FAC9
  106      AL11  =FAC1*XAA(15,I)*0.029
  107      AL21  =0.0
  108      AL31  =FAC3*XAA(21,I)
  109      AL41  =FAC4*XAA(17,I)*0.008
  110      AL91  =FAC9*XAA(1  ,I)
  111      AL141  =FAC14*XAA(2  ,I)
  112      AL191  =FAC19*XAA(5  ,I)
  113      ALFAE=0.0
  114      ALFA2  =AL11*FRS+AL21+AL31+AL41*FRCNR+AL141+ALFAE+AL91+AL191
  115  C
  116  C     CORRECTION FOR INDUCED EMISSION
```

```
CARD
NUMBER
  117      C
  118            ALFA(2,I)=(1.+1.667*T*(EXP(-1.0/T)-EXP(-0.4/T)))*ALFA2
  119      C
  120            WRITE(NWRITE,202) ALFA2,ALFA(2,I)
  121        202 FORMAT(/,14X,2HO2,10X,14HO0.40 TO 01.00,18X,2G12.5,/)
  122      C
  123      C     BAND  3 CALCULATIONS, FREQUENCY =  1.00 TO  2.00 ELECTRON VOLTS
  124      C
  125            FAC1=(1.86E-16*EXP(-1.2/T))
  126            FAC2=0.0
  127            FAC3=(7.04E-17*EXP(-7.18/T))
  128            FAC4=4.0E-17
  129            FAC14=5.5E-16*EXP(-10.7/T)
  130            FAC9=4.0E-16*T*EXP(-12.8/T)
  131            FAC10=FAC9
  132            AL11  =FAC1*XAA(15,I)*0.029
  133            AL21  =0.0
  134            AL31  =FAC3*XAA(21,I)
  135            AL41  =FAC4*XAA(17,I)*0.008
  136            AL91  =FAC9*XAA(1  ,I)
  137            AL141  =FAC14*XAA(2  ,I)
  138            AL191  =FAC19*XAA(6  ,I)
  139            ALFAE=0.0
  140            ALFA3  =AL11*FRS+AL21+AL31+AL41*FRCNR+AL141+ALFAE+AL91+AL191
  141      C
  142      C     CORRECTION FOR INDUCED EMISSION
  143      C
  144            ALFA(3,I)=(1.+1.00*T*(EXP(-2.0/T)-EXP(-1.0/T)))*ALFA3
  145      C
  146            WRITE(NWRITE,203) ALFA3,ALFA(3,I)
  147        203 FORMAT(/,14X,2HO3,10X,14HO1.00 TO 02.00,18X,2G12.5,/)
  148      C
  149      C     BAND  4 CALCULATIONS, FREQUENCY =  2.00 TO  3.40 ELECTRON VOLTS
  150      C
  151            FAC1=7.5E-17
  152            FAC5=3.34E-18*EXP(-0.29/T)
  153            FAC6=3.26E-18*EXP(-0.65/T)
  154            FAC3=2.06E-17*EXP(-6.11/T)
  155            FAC7=7.8E-17
  156            FAC4=1.0E-16
  157            FAC4V=3.7E-17
  158            FAC14=5.93E-17*EXP(-9.55/T)
  159            AL32=FAC3*XAA(21,I)
  160            AL12  =FAC1*XAA(15,I)*0.029
  161            AL72  =FAC7*XAA(18,I)*0.13
  162            AL52  =FAC5*XAA(15,I)*0.05
  163            AL62  =FAC6*XAA(15,I)*0.06
  164            AL42  =FAC4*XAA(17,I)*0.008
  165            AL4V2  =FAC4V*XAA(17,I)*0.027
  166            AL142  =FAC14*XAA(2  ,I)
  167            ALFA4  =AL12*FRS+AL32+AL42*FRCNR+AL4V2*FRCNV+AL52*FRFH+AL62*FRD+
  168           1AL72*FR3L+AL142
  169      C
  170      C     CORRECTION FOR INDUCED EMISSION
  171      C
  172            ALFA(4,I)=(1.+0.715*T*(EXP(-3.4/T)-EXP(-2.0/T)))*ALFA4
  173      C
  174            WRITE(NWRITE,204) ALFA4,ALFA(4,I)
```

```
CARD
NUMBER
  175      204 FORMAT(/,14X,2HO4,10X,14HO2.00 TO 03.40,18X,2G12.5,/)
  176C
  177C       BAND  5 CALCULATIONS, FREQUENCY =   3.40 TO   5.20 ELECTRON VOLTS
  178C
  179        FAC1=3.19E-18*EXP(-0.27/T)
  180        FAC5=2.44E-17
  181        FAC6=1.31E-17*EXP(-.79/T)
  182        FAC8=2.41E-16*EXP(-1.52/T)
  183        FAC9=3.38E-17*EXP(-10.2/T)
  184        FAC3=3.36E-18*EXP(-3.44/T)
  185        FAC10=2.09E-17
  186        FAC11=3.0E-17
  187        FAC4=3.7E-18
  188        FAC14=1.8E-17*EXP(-8.75/T)
  189        AL15 = FAC1*XAA(15,I)*0.029
  190        AL33 =FAC5*XAA(15,I)*0.05
  191        AL63 =FAC6*XAA(15,I)*0.06
  192        AL93 =FAC9*XAA(1 ,I)
  193        AL33 =FAC3*XAA(21,I)
  194        AL103 =FAC10*XAA(23,I)*0.19
  195        AL113 =FAC11*XAA(20,I)
  196        AL83 =FAC8*XAA(15,I)*0.02
  197        AL43 =FAC4*XAA(17,I)*0.027
  198        AL143 =FAC14*XAA(2 ,I)
  199        ALFA5 =AL13*FRS+AL53*FRF+AL63*FRC+AL83*FRF+AL93*AL33*AL103*FRA+
  200       1AL113+AL63*FRCAV+AL143
  201C
  202C       CORRECTION FOR INDUCED EMISSION
  203C
  204        ALFA(5,I)=(1.+0.555*T*(EXP(-5.2/T)-EXP(-3.4/T)))*ALFA5
  205C
  206        WRITE(NWRITE,205) ALFA5     ,ALFA(5,I)
  207  205 FORMAT(/,14X,2HO5,10X,14HO3.40 TO 05.20,18X,2G12.5,/)
  208C
  209C       BAND  6 CALCULATIONS, FREQUENCY =   5.20 TO   6.80 ELECTRON VOLTS
  210C
  211        FAC6=4.5E-16*EXP(-1.17/T)
  212        FAC8=3.98E-16*EXP(-0.72/T)
  213        FAC12=1.51E-17
  214        FAC13=3.32E-18*EXP(-1.6/T)
  215        FAC9=1.19E-17*EXP(-10.2/T)
  216        FAC3=1.69E-17*EXP(-2.63/T)
  217        FAC10=2.69E-17
  218        FAC11=2.0E-17
  219        FAC14=9.9E-18*EXP(-8.35/T)
  220        FAC15=1.0E-18
  221        FAC7=4.5E-18
  222        AL74=FAC7*XAA(18,I)
  223        AL54 =FAC5*XAA(15,I)*0.06
  224        AL84 =FAC8*XAA(15,I)*0.02
  225        AL124 =FAC12*XAA(15,I)*0.10
  226        AL134 =FAC13*XAA(13,I)*0.19
  227        AL94 =FAC9*XAA(1 ,I)
  228        AL34 =FAC3*XAA(21,I)
  229        AL104 =FAC10*XAA(23,I)*0.19
  230        AL114 =FAC11*XAA(20,I)
  231        AL144 =FAC14*XAA(2 ,I)
  232        AL154 =FAC15*XAA(14,I)
```

```
CARD
NUMBER
  233       ALFA6  =AL64*FR6+AL84*FR8+AL124*FR4+AL134*FR4P+AL94+AL34+AL14*FRAX
  234      1+AL114+AL144+AL154+AL74*FR3V
  235 C
  236 C     CORRECTION FOR INDUCED EMISSION
  237 C
  238       ALFA(6,I)=(1.+0.625*T*(EXP(-6.8/T)-EXP(-5.2/T)))*ALFA6
  239 C
  240       WRITE(NWRITE,206) ALFA6,ALFA(6,I)
  241   206 FORMAT(/,14X,2HO6,10X,14HO5.20 TO 06.80,18X,2G12.5,/)
  242 C
  243 C     BAND  7 CALCULATIONS, FREQUENCY =  6.80 TO  8.60 ELECTRON VOLTS
  244 C
  245       FAC13=5.5E-18
  246       FAC9=5.55E-18*EXP(-10.2/T)
  247       FAC14=3.2E-18*EXP(-3.77/T)
  248       FAC3=7.61E-17*EXP(-0.952/T)
  249       FAC15=2.5E-18
  250       AL135 =FAC13*XNN(13,I)*0.19
  251       AL95  =FAC9*XNN(1  ,I)
  252       AL145 =FAC14*XNN(2  ,I)
  253       AL35  =FAC3*XNN(21,I)
  254       AL155 =FAC15*XNN(14,I)
  255       ALFA7 =AL135*FR4F+AL95+AL145+AL35+AL155
  256 C
  257 C     CORRECTION FOR INDUCED EMISSION
  258 C
  259       ALFA(7,I)=(1.+0.555*T*(EXP(-8.6/T)-EXP(-6.8/T)))*ALFA7
  260 C
  261       WRITE(NWRITE,207) ALFA7     ,ALFA(7,I)
  252   207 FORMAT(/,14X,2HO7,10X,14HO6.80 TO 08.60,18X,2G12.5,/)
  263 C
  264 C     BAND  9 CALCULATIONS, FREQUENCY =  8.60 TO 10.00 ELECTRON VOLTS
  265 C
  266       FAC13=6.00E-18
  267       FAC9=3.09E-18*EXP(-10.2/T)
  268       FAC14=3.9E-18*EXP(-2.86/T)
  269       FAC3=3.89E-18*EXP(-0.177/T)
  270       FAC15=2.5E-18
  271       AL136 =FAC13*XNN(13,I)*0.19
  272       AL96  =FAC9*XNN(1, I)
  273       AL146 =FAC14*XNN(2  ,I)
  274       AL36  =FAC3*XNN(21,I)
  275       AL156 =FAC15*XNN(14,I)
  276       ALFA8 =AL136*FR4F+AL96+AL146+AL36+AL156
  277 C
  278 C     CORRECTION FOR INDUCED EMISSION
  279 C
  280       ALFA(8,I)=(1.+0.715*T*(EXP(-10.0/T)-EXP(-8.6/T)))*ALFA8
  281 C
  282       WRITE(NWRITE,208) ALFA8,ALFA(8,I)
  283   208 FORMAT(/,14X,2HO8,10X,14HO8.60 TO 10.00,18X,2G12.5,/)
  284 C
  285 C     BAND  9 CALCULATIONS, FREQUENCY = 10.00 TO 11.20 ELECTRON VOLTS
  286 C
  287       FAC13=5.65E-19*EXP(-0.46/T)
  288       FAC9=2.1E-18*EXP(-10.2/T)
  289       FAC14=8.2E-18*EXP(-1.18/T)
  290       FAC3=1.34E-18*EXP(-0.187/T)
```

```
CARD
NUMBER
  291       FAC15=2.5E-18
  292       AL137 =FAC13*XNN(13,I)*0.1
  293       AL97 =FAC9*XNN(1  ,I)
  294       AL147 =FAC14*XNN(2  ,I)
  295       AL37 =FAC3*XNN(21,I)
  296       AL157 =FAC15*XNN(14,I)
  297       ALFA9=AL137*FRAC+AL97+AL147+AL37+AL157
  298 C
  299 C     CORRECTION FOR INDUCED EMISSION
  300 C
  301       ALFA(9,I)=(1.+0.833*T*(EXP(-11.2/T)-EXP(-10.0/T)))*ALFA9
  302 C
  303       WRITE(NWRITE,209) ALFA9    ,ALFA(9,I)
  304   209 FORMAT(/,14X,2HA9,10X,14H10.00 TO 11.20,18X,2G12.5,/)
  305 C
  306 C     BAND 10 CALCULATIONS, FREQUENCY =  11.20 TO 13.60 ELECTRON VOLTS
  307 C
  308       FAC9=1.32E-18*EXP(-10.2/T)
  309       FAC15=5.0E-18
  310       FAC14=1.4E-17*EXP(-0.178/T)
  311       FAC3=2.38E-18*EXP(-0.166/T)
  312       AL98 =FAC9*XNN(1  ,I)
  313       AL158 =FAC15*XNN(14,I)
  314       AL148 =FAC14*XNN(2  ,I)
  315       AL38 =FAC3*XNN(21,I)
  316       ALFA10=AL98+AL158+AL148+AL38
  317 C
  318 C     CORRECTION FOR INDUCED EMISSION
  319 C
  320       ALFA(10,I)=(1.+0.417*T*(EXP(-13.6/T)-EXP(-11.2/T)))*ALFA10
  321 C
  322       WRITE(NWRITE,210) ALFA10,ALFA(10,I)
  323   210 FORMAT(/,14X,2HA10,10X,14H11.20 TO 13.60,18X,2G12.5,/)
  324 C
  325 C     BAND 11 CALCULATIONS, FREQUENCY =  13.60 TO 19.00 ELECTRON VOLTS
  326 C
  327       FAC16=1.0E-17
  328       FAC17=4.85E-18
  329       FAC14=1.4E-17*EXP(-0.178/T)
  330       FAC3=2.64E-18*EXP(-.31/T)
  331       FAC18=0.0
  332       FAC19=3.5E-18
  333       AL199 =FAC19*XNN(6  ,I)
  334       AL169 =FAC16*XNN(13,I)
  335       AL179 =FAC17*XNN(1  ,I)
  336       AL149 =FAC14*XNN(2  ,I)
  337       AL39  =FAC3*XNN(21,I)
  338       AL189 =FAC18*XNN(3  ,I)
  339       ALFA11=AL169*FRAC+AL179+AL149+AL39+AL189+AL199
  340 C
  341 C     CORRECTION FOR INDUCED EMISSION
  342 C
  343       ALFA(11,I)=(1.+0.185*T*(EXP(-19.0/T)-EXP(-13.6/T)))*ALFA11
  344 C
  345       WRITE(NWRITE,211) ALFA11   ,ALFA(11,I)
  346   211 FORMAT(/,14X,2HA11,10X,14H13.60 TO 19.00,18X,2G12.5,/)
  347 C
  348 C     BAND 12 CALCULATIONS, FREQUENCY =  19.00 TO 24.40 ELECTRON VOLTS
```

```
C
      FAC16=1.7E-17
      FAC17=2.0E-18
      FAC14=1.4E-17*EXP(-0.179/T)
      FAC3=2.9E-18*EXP(-0.487/T)
      FAC19=4.2E-13*EXP(-23.6/T)
      FAC10=3.5E-18
      AL1610 =FAC16*XAN(13,I)
      AL1710 =FAC17*XAN(1 ,I)
      AL1410 =FAC14*XAN(2 ,I)
      AL310  =FAC3*XAN(21,I)
      AL1810 =FAC18*XAN(3 ,I)
      AL1910 =FAC19*XAN(6 ,I)
      ALFA12 =AL1610*FRPH+AL1710+AL1410+AL310+AL1810+AL1910
C
C     CORRECTION FOR INDUCED EMISSION
C
      ALFA(12,I)=(1.+0.185*T*(EXP(-24.4/T)-EXP(-19.0/T)))*ALFA12
C
      WRITE(NWRITE,212) ALFA12,ALFA(12,I)
  212 FORMAT(//,14X,2H12,10X,14H19.09 TO 24.40,18X,2G12.5,/)
C
      ALFAB1(I)=(ALFA(1,I)*0.3+ALFA(2,I)*0.6+ALFA(3,I)*1.0+ALFA(4,I)*1.4
     * +ALFA(5,I)*1.8+ALFA(6,I)*1.6+ALFA(7,I)*1.8+ALFA(8,I)*1.4+ALFA(9,I
     *)*1.2)/11.1
      ALFAB2(I)=(ALFA(10,I)*2.4+ALFA(11,I)*5.4+ALFA(12,I)*5.4)/13.2
      WRITE(NWRITE,500)ALFAB1(I),ALFAB2(I)
  500 FORMAT(//,10X,41H2-BAND MODEL WITH PEAK AT 1100 ANGSTROMS,//,
     1 10X,33HIR-BAND ABSORPTION COEFFICIENT = ,1G12.5,5X,33HUV-BAND ABS
     2ORPTION COEFFICIENT = ,1G12.5,/)
C
C     COMPUTE PLANCK AND ROSSELAND MEAN ABSORPTION COEFFICIENTS
C
      HV1=0.10
      HV2=0.40
      CALL PLANCK(HV1,HV2,TK     ,QUADND,QUAD,K)
      PLKM1 =ALFA(1 ,I)*QUADND
      CALL ROSSEL(HV1,HV2,TK,QUADND,QUAD,KK)
      ROSL1 =(1./ALFA(1 ,I))*QUADND
      HV1=HV2
      HV2=1.0
      CALL PLANCK(HV1,HV2,TK     ,QUADND,QUAD,K)
      PLKM2 =ALFA(2 ,I)*QUADND
      CALL ROSSEL(HV1,HV2,TK,QUADND,QUAD,KK)
      ROSL2 =(1./ALFA(2 ,I))*QUADND
      HV1=HV2
      HV2=2.0
      CALL PLANCK(HV1,HV2,TK     ,QUADND,QUAD,K)
      PLKM3 =ALFA(3 ,I)*QUADND
      CALL ROSSEL(HV1,HV2,TK,QUADND,QUAD,KK)
      ROSL3 =(1./ALFA(3 ,I))*QUADND
      HV1=HV2
      HV2=3.4
      CALL PLANCK(HV1,HV2,TK     ,QUADND,QUAD,K)
      PLKM4 =ALFA(4 ,I)*QUADND
      CALL ROSSEL(HV1,HV2,TK,QUADND,QUAD,KK)
      ROSL4 =(1./ALFA(4 ,I))*QUADND
      HV1=HV2
```

```
CARD
NUMBER
 407          HV2=5.2
 408          CALL PLANCK(HV1,HV2,TK      ,QUADND,QUAD,K)
 409          PLKP5 =ALFA(5  ,I)*QUADND
 410          CALL RCSSEL(HV1,HV2,TK,QUADND,QUAD,KK)
 411          RCSL5 =(1./ALFA(5  ,I))*QUADND
 412          HV1=HV2
 413          HV2=6.8
 414          CALL PLANCK(HV1,HV2,TK      ,QUADND,QUAD,K)
 415          PLKP6 =ALFA(6  ,I)*QUADND
 416          CALL RCSSEL(HV1,HV2,TK,QUADND,QUAD,KK)
 417          RCSL6 =(1./ALFA(6  ,I))*QUADND
 418          HV1=HV2
 419          HV2=8.6
 420          CALL PLANCK(HV1,HV2,TK      ,QUADND,QUAD,K)
 421          PLKP7 =ALFA(7  ,I)*QUADND
 422          CALL RCSSEL(HV1,HV2,TK,QUADND,QUAD,KK)
 423          RCSL7 =(1./ALFA(7  ,I))*QUADND
 424          HV1=HV2
 425          HV2=10.0
 426          CALL PLANCK(HV1,HV2,TK      ,QUADND,QUAD,K)
 427          PLKP8 =ALFA(8  ,I)*QUADND
 428          CALL RCSSEL(HV1,HV2,TK,QUADND,QUAD,KK)
 429          RCSL8 =(1./ALFA(8  ,I))*QUADND
 430          HV1=HV2
 431          HV2=11.2
 432          CALL PLANCK(HV1,HV2,TK      ,QUADND,QUAD,K)
 433          PLKP9 =ALFA(9  ,I)*QUADND
 434          CALL RCSSEL(HV1,HV2,TK,QUADND,QUAD,KK)
 435          RCSL9 =(1./ALFA(9  ,I))*QUADND
 436          HV1=HV2
 437          HV2=13.6
 438          CALL PLANCK(HV1,HV2,TK      ,QUADND,QUAD,K)
 439          PLKP10=ALFA(10,I)*QUADND
 440          CALL RCSSEL(HV1,HV2,TK,QUADND,QUAD,KK)
 441          RCSL10=(1./ALFA(10,I))*QUADND
 442          HV1=HV2
 443          HV2=19.0
 444          CALL PLANCK(HV1,HV2,TK      ,QUADND,QUAD,K)
 445          PLKP11=ALFA(11,I)*QUADND
 446          CALL RCSSEL(HV1,HV2,TK,QUADND,QUAD,KK)
 447          RCSL11=(1./ALFA(11,I))*QUADND
 448          HV1=HV2
 449          HV2=24.4
 450          CALL PLANCK(HV1,HV2,TK      ,QUADND,QUAD,K)
 451          PLKP12=ALFA(12,I)*QUADND
 452          CALL RCSSEL(HV1,HV2,TK,QUADND,QUAD,KK)
 453          RCSL12=(1./ALFA(12,I))*QUADND
 454          PLKPA(I)=PLKP1+PLKP2+PLKP3+PLKP4+PLKP5+PLKP6+PLKP7+
 455         1PLKP8+PLKP9+PLKP10+PLKP11+PLKP12
 456          RCSSL(I)=25.974/(RCSL1+RCSL2+ROSL3+ROSL4+ROSL5+ROSL6+
 457         1RCSL7+ROSL8+RCSL9+RCSL10+ROSL11+ROSL12)
 458          WRITE(NWRITE,102) PLKPA(I),RCSSL(I)
 459      102 FORMAT(/,10X,14HPLANCK MEAN = ,G12.5,5X,17HROSSELAND MEAN = ,
 460         1 G12.5,//)
 461        6 CONTINUE
 462          GO TO 1
 463          END
 464          SUBROUTINE FEPP (NT,AS,NYY,NERR,I)
```

```
CARD
NUMBER
  465
  466
  467
  468
  469
  470
  471
  472
  473
  474
  475
  476
  477
  478
  479
  480
  481
  482
  483
  484
  485
  486
  487
  488
  489
  490
  491
  492
  493
  494
  495
  496
  497
  498
  499
  500
  501
  502
  503
  504
  505
  506
  507
  508
  509
  510
  511
  512
  513
  514
  515
  516
  517
  519
  519
  520
  521
  522
C
C     DUMMY FEMP SUBROUTINE
C
      COMMON/TABLES/ ST(25,100),TT(100),TEE(100),XAN(25,100),
     1 ALFA(12,100),ALFAB1(100),ALFAB2(100),G(100),F(100),RHO(100)
C
      NWRITE=6
      DO 30 J=1,AS
      DO 10 M=1,AT
      IF(TEE(I)-TT(M)) 20,10,10
   10 CONTINUE
      M=AT
   20 M=M-1
      K=M+1
      SL=(ST(J,K)-ST(J,M))/(TT(K)-TT(M))
      YY=SL*(TEE(I)-TT(M))+ST(J,M)
      XAN(J,I)=10.**YY
      IF(XAN(J,I) .EQ. 1.0) XAN(J,I)=0.0
   30 CONTINUE
      RETURN
      END
      SUBROUTINE PLANCK(HV1,HV2,TK,PLINC,PLINT,K)
C
C     COMPUTATION OF INTEGRAL IN DEFINITION OF PLANCK MEAN ABSORPTION
C     COEFFICIENT
C
      K=0
      T=TK*1.8
      X1=(1.24/HV2)*T
      X2=(1.24/HV1)*T
      CON=6.9253E+16/(25896.**4)
      PLIAD1=0.0
      PLIAD2=0.0
      IF(X1 .LE. 7400. .AND. X2 .LE. 7400.) GO TO 10
      IF(X1 .GT. 7400. .AND. X2 .GT. 7400.) GO TO 20
      K=1
      Y2=25896./7400.
      GO TO 11
   10 Y2=25896./X2
   11 Y1=25896./X1
      PLIAD1=CON*(EXP(-Y2)*(Y2**3+3.0*(Y2**2)+6.0*Y2+6.0)-(EXP(-Y1)*((Y1
     1**3)+3.0*(Y1**2)+6.0*Y1+6.0)))
      IF(K .EQ. 0) GO TO 40
      X1=7400.
   20 A=2.231
      B=-1.473E-04
      C=0.5
      PLIAD2=((1.-A*EXP(B*X2))**C)-((1.-A*EXP(B*X1))**C)
   40 PLIAD=PLIAD2+PLIAD1
      PLINT=5.668E-12*(TK**4)*PLINC
      RETURN
      END
      SUBROUTINE ROSSEL(HV1,HV2,TK,ROSNCT,ROSINT,KK)
C
C     COMPUTATION OF INTEGRAL IN DEFINITION OF ROSSELAND MEAN ABSORPTION
C     COEFFICIENT
C
      KK=0
```

```
CARD
NUMBER
  523                T=TK/11606.
  524                X1=HV1/T
  525                X2=HV2/T
  526                RCSAD1=0.
  527                RCSAD2=0.
  528                IF(X1 .LE. 3.7 .AND. X2 .LE. 3.7) GO TO 10
  529                IF(X1 .GT. 3.7 .AND. X2 .GT. 3.7) GO TO 20
  530                KK=1
  531                Y2=X2
  532                X2=3.7
  533             10 RCSAD1=0.334306*(X2**3-X1**3)-0.013544*(X2**5-X1**5)-3.5E029E-03*(
  534               1X2**6-X1**6)+2.20336F-03*(X2**7-X1**7)-2.5666CE-04*(X2**8-X1**8)
  535                IF(KK .EQ. 0) GO TO 40
  536                X2=Y2
  537                X1=3.7
  538             20 RCSAD2=-EXP(-X2)*(X2**4+4.*(X2**3)+12.*(X2**2)+24.*X2+24.)+
  539               1         EXP(-X1)*(X1**4+4.*(X1**3)+12.*(X1**2)+24.*X1+24.)
  540             40 RCSADT=RCSAD1+RCSAD2
  541                RCSIAT=RCSADT*1.403E-11*(TK**3)
  542                RETURN
  543                END

**** E N D  O F  D A T A ****

/*
```

APPENDIX B

Radiation equations

The one-dimensional equations have been derived in a number of sources (Ref 2, 3, 48, 78, 79). The basic equation is:

$$\mu \frac{dI_\nu}{ds} = \alpha_\nu \left(\frac{e_{b_\nu}(T)}{\pi} - I_\nu \right) \tag{B-1}$$

where

μ = $\cos \theta$

α_ν monochromatic absorption coefficient

e_{b_ν} = Planck radiation function = $\dfrac{2\pi\nu^3}{c^2(e^{h\nu/kT} - 1)}$

I_ν = monochromatic intensity

s = arc length

which becomes upon introducing

$$\tau_\nu \equiv \int_0^s \alpha_\nu \, d\xi \quad , \tau_{o_\nu} \equiv \int_0^{s_o} \alpha_\nu \, d\xi \tag{B-2}$$

$$\mu \frac{dI_\nu}{d\tau_\nu} = \frac{e_{b_\nu}}{\pi} - I_\nu \tag{B-3}$$

For a non-scattering medium and a diffuse wall (lower surface) and a transparent shock (upper surface) when there is an external source at the shock (subscript 2) which has both a diffuse component, $q^R_{x_{d_2}}$, and a parallel component, $q^R_{x_{p_2}}$ at an angle $\cos^{-1}\mu_o$, as was formulated by Viskanta and Merriam (Ref 80), the flux is:

$$q^R_\nu = 2B_{1_\nu} E_3(\tau_\nu) - 2q^R_{x_{d_\nu}} E_3(\tau_{o_\nu} - \tau_\nu) - \mu_o q^R_{x_{p_\nu}} e^{-(\tau_{o_\nu} - \tau_\nu)/\mu_o} + 2\int_0^{\tau_\nu} e_{b_\nu}(t) E_2(\tau_\nu - t)\, dt - 2\int_0^{\tau_{o_\nu}} e_{b_\nu}(t) E_2(\tau_\nu - t)\, dt \qquad \text{(B-4)}$$

Taking the derivative with respect to the optical depth, τ_ν of (B-4), one obtains:

$$-\frac{dq^R_\nu}{d\tau_\nu} = 2B_{1_\nu} E_2(\tau_\nu) + 2q^R_{x_{d_\nu}} E_2(\tau_{o_\nu} - \tau_\nu) + q^R_{x_{p_\nu}} e^{-(\tau_{o_\nu} - \tau_\nu)/\mu_o} + 2\int_0^{\tau_{o_\nu}} e_{b_\nu}(t) E_1(|\tau_\nu - t|)\, dt - 4e_{b_\nu}(\tau_\nu) \qquad \text{(B-5)}$$

Now in the combined diffuse and parallel case (Ref 42)

$$B_{1_\nu} = \varepsilon_1 e_{b_\nu} + 2(1 - \varepsilon_1) q^R_{x_{d_\nu}} E_3(\tau_o) + 1/2\, \mu_o q^R_{x_{p_\nu}} e^{-\tau_o/\mu_o} + \int_0^{\tau_{o_\nu}} e_{b_\nu}(t) E_2(t)\, dt \qquad \text{(B-6)}$$

The ablation layer model assumes that surface 1 is black and has already assumed that surface 2 is transparent. It will now be assumed that the external source consists of primarily diffuse radiation ($q^R_{x_{d_\nu}} >> q^R_{x_{p_\nu}}$). Therefore, set $q^R_{x_{p_\nu}} = 0$. The physical situation of cool walls and an air shock layer with a high temperature external source makes it reasonable to neglect B_{1_ν} with respect to $q^R_{x_{d_\nu}}$. Then

$$q^R_\nu = 2 \int_0^{\tau_\nu} e_{b_\nu}(t) E_2(\tau_\nu - t)\, dt - 2 \int_0^{\tau_{o_\nu}} e_{b_\nu}(t)\, E_2(t - \tau_\nu)\, dt +$$

$$- 2q^R_{x_{d_\nu}} E_3(\tau_{o_\nu} - \tau_\nu) \qquad \text{(B-7)}$$

and

$$-\frac{dq^R}{d\tau_\nu} = 2 \int_0^{\tau_{o_\nu}} e_{b_\nu}(t)\, E_1(|\tau_\nu - t|)\, dt + 2q^R_{x_{d_\nu}} E_2(\tau_{o_\nu} - \tau_\nu) +$$

$$- 4e_{b_\nu}(\tau_\nu) \qquad \text{(B-8)}$$

Now transforming to physical coordinates

$$\frac{dq^R_\nu}{dy} = \frac{dq^R_\nu}{d\tau_\nu} \cdot \frac{d\tau_\nu}{dy} \qquad \text{(B-9)}$$

or from the definition of τ_ν

$$\frac{dq_\nu^R}{dy} = \alpha_\nu \frac{dq_\nu^R}{d\tau_\nu} \tag{B-10}$$

The flux at the wall ($\tau_\nu = 0$) is:

$$q_\nu^R(0) = e_{b_\nu}(0) - 2\int_0^{\tau_{\nu_o}} e_{b_\nu}(t)\, E_2(t)\, dt \tag{B-11}$$

Integrating over frequency, (B-8) and (B-10) lead to:

$$-\frac{dq^R}{dy} = 2\int_{\nu=0}^{\infty} \alpha_\nu \int_0^{\tau_{\nu_o}} e_{b_\nu}(t)\, E_1(|\tau_\nu - t|)\, dt\, d\nu +$$

$$+ 2\int_{\nu=0}^{\infty} \alpha_\nu\, q_{x_{d_\nu}}^R\, E_2(\tau_{o_\nu} - \tau_\nu)\, d\nu +$$

$$- 4\int_{\nu=0}^{\infty} \alpha_\nu\, e_{b_\nu}(\tau_\nu)\, d\nu \tag{B-12}$$

Throughout the above:

$$E_n(t) = \int_0^1 \gamma^{n-2}\, e^{-t/\gamma}\, d\gamma$$

and

$$\alpha_\nu = \alpha'_\nu \left(1 - e^{-h\nu/kT}\right)$$

where E_n is the exponential integral of order n and α_ν is the spectral absorption coefficient corrected for induced emission.

APPENDIX C

Conical body analysis

In order to arrive at a method for calculating the flow about a conical body undergoing massive ablation, it is necessary to examine the flow shown in Figure C1. The flow between the shock and the body can be divided into three separate regions. These are the inviscid flow near the surface, a free shear layer, and an outer inviscid region. Examination of the shear layer shows that it has the following characteristics:

1. it acts as a transition region between the two inviscid flows for temperature, velocity, density, and species concentration. Therefore, these properties will change appreciably across it;

2. it has a thickness of the order of an ordinary boundary layer. That requires, then, that it be a relatively thin layer for large Reynolds numbers;

3. the change in pressure across its thickness can be taken as a first approximation to be constant as it is done in boundary layer theory;

4. due to its small thickness, it only slightly influences radiation transport, i.e., no appreciable absorption.

These facts are extremely important since they in essence show that as a first approximation one can neglect the thickness of the shear layer and consider it simply as a line of discontinuity of density, temperature, velocity, and concentration, across which the pressure will be continuous. The problem of calculating the radiation-coupled aerodynamic flow then reduces to calculating two inviscid flow regions between the shock and the body which are separated by a line across which the pressure is continuous (see Fig C2).

The inviscid Region I near the body will be essentially pure ablation products, while Region II will contain none. Both the temperature and velocity of Region I will be substantially lower than those of Region II. These are important facts to note since they indicate that previous estimates based on the free stream velocity and temperature can be substantially in error, a point that most investigators have not realized.

A. Model for Region I

The existing model uses the equations describing the inviscid flow about the cone. If we write them in coordinates normal, y, and tangent, x, to the cone as shown in Figure C2, they become for a local cone radius r and a cone half-angle θ:

Continuity Equation

$$\frac{\partial (\rho u r)}{\partial x} + \frac{\partial (\rho v r)}{\partial y} = 0 \qquad \text{(C1)}$$

Momentum Equations (neglecting radiation pressure)

$$\frac{\partial}{\partial x}\left[(p + \rho u^2) r \right] + \frac{\partial}{\partial y} (\rho u v r) - p \sin\theta = 0 \qquad \text{(C2)}$$

$$\frac{\partial}{\partial x} (\rho u v r) + \frac{\partial}{\partial y}\left[(p + \rho v^2) r \right] - p \cos\theta = 0 \qquad \text{(C3)}$$

Energy Equation (neglecting radiation pressure effects)

$$\frac{\partial}{\partial x}\left[\rho u r \left(h + \frac{u^2 + v^2}{2}\right) \right] + \frac{\partial}{\partial y}\left[\rho v r \left(h + \left(\frac{u^2 + v^2}{2}\right)\right) \right] = -\nabla \cdot \vec{q}_R$$

$$- \frac{\partial}{\partial x}(rup) - \frac{\partial}{\partial y}(rvp) \qquad \text{(C4)}$$

Equation of State

$$p = Z \rho R T \qquad \text{(C5)}$$

and

Radiation Transport Equation (neglecting scattering)

$$\frac{dI_\nu}{ds} = \alpha_\nu \left[B_\nu(T) - I_\nu \right] \qquad \text{(C6)}$$

A very important simplification obtained from this model is that we do not need species equations since Region I is almost pure ablation products and Region II is pure fireball products. The species equations would be required if one studied the shear layer. For our purposes, however, we can avoid this difficulty since the shear layer does not significantly affect the radiation transport.

It is well known that in the energy equation the radiation term is given by:

$$\vec{q}_R = 4\pi \int_\nu \alpha_\nu B_\nu(T) d\nu - \int_\nu \int_\Omega \alpha_\nu I_\nu d\Omega d\nu \qquad \text{(C7)}$$

The principle difficulty in numerically integrating the transport equations lies in this term. This is due to the dependence of I_ν on the solid angle Ω as well as the coordinates x and y. We seek therefore a simplification which will reduce this difficulty. As a first step, one would like to treat the radiation transport as one-dimensional, i.e., as a function of y alone at a given x. The conditions for which such an approximation can be expected to be valid are now examined.

This approximation would be expected to be reasonable if the vapor layer thickness is small compared with the characteristic absorption length of the vapor (optically thin case). An equivalent physical viewpoint is that we would expect the energy transport in the normal direction to the surface, i.e., y, to be the dominant effect, and radiation transport in the x direction a second-order one.

Now writing the equation for the radiation intensity I_ν in the x, y coordinates it can be shown that these statements are borne out mathematically. Then:

$$\frac{dI_\nu}{ds} = \frac{dx}{ds}\frac{\partial I_\nu}{\partial x} + \frac{dy}{ds}\frac{\partial I_\nu}{\partial y} = \alpha_\nu \left[B_\nu(T) - I_\nu \right] \qquad \text{(C8)}$$

Next introducing the dimensionless variables,

$$\bar{x} \equiv \frac{\int_0^x \alpha_\nu \, dx}{\ell \, \alpha_{\nu_{max}}} \; ; \; \bar{y} \equiv \frac{\int_0^y \alpha_\nu \, dy}{\delta_{max} \, \alpha_{\nu_{max}}} \quad \bar{I}_\nu \equiv \frac{I_\nu}{I_{\nu_{max}}} \; ;$$

$$B_\nu \equiv \frac{B_\nu (T)}{I_{\nu_{max}}}$$

the resulting equation is

$$\frac{dx}{ds} \frac{\delta_{max}}{\ell} \frac{\partial \bar{I}_\nu}{\partial \bar{x}} + \frac{dy}{ds} \frac{\partial \bar{I}_\nu}{\partial \bar{y}} = \delta_{max} \, \alpha_{\nu_{max}} \left[\bar{B}_\nu - \bar{I}_\nu \right] \qquad (C9)$$

The maximum values of I_ν, the radiation intensity, and α_ν, the absorption coefficient, were chosen to make the dimensionless variables less than one. Note also the ℓ denotes the maximum value of x and δ_{max} the maximum thickness of the ablation product layer. Noting now that dx/ds and dy/ds are direction cosines and have a maximum value of one, it is clear that if $(\delta_{max}/\ell) << 1$ the $\partial \bar{I}_\nu / \partial \bar{x}$ term can be neglected, as a first approximation, with respect to the $\partial \bar{I}_\nu / \partial \bar{y}$ term. It is expected now that this criterion will hold in most physical problems of interest.

The energy equation can then be written as:

$$\frac{\partial}{\partial x} \left[\rho u r \left(h + \frac{u^2 + v^2}{2} \right) \right] + \frac{\partial}{\partial y} \left[\rho v r \left(h + \frac{u^2 + v^2}{2} \right) \right] +$$

$$+ \frac{\partial}{\partial y} (\rho u r) + \frac{\partial}{\partial y} (\rho v r) + \frac{\partial q^R}{\partial y} = 0 \qquad (C10)$$

Equations (C1), (C2), (C3), (C5), and (C10) are now a complete mathematical formulation and description of the radiation and flow

field in Region I. The specifications of the boundary conditions for Region I are now required.

Boundary Conditions for Region I

At the surface of the body, the conditions are as follows:

$$\dot{m} = \rho_w v_w = \frac{q^R \left[0, T_w, \delta(x)\right]}{\Delta H_{eff}} ;$$

$$u = 0 \text{ ; and } T_w = T_{ablation}$$

q^R is the radiation flux of equation (C7) evaluated at the wall and ΔH_{eff} is the heat of vaporization of the surface. At the contact surface the conditions can be defined as:

$$\text{at } y = \delta(x) \qquad p_{\text{Region I}} = p_{\text{Region II}}$$

$$v_{\text{Region I}} = v_{\text{Region II}} = 0$$

B. Region II

Region II in the model requires little explanation except to say that it is a classical inviscid flow region described by Euler's equations of flow, which can be calculated using existing flow field programs. The only unknown for this region is the position of the boundary $\delta(x)$. Therefore Region I and Region II will have to be solved simultaneously since they are coupled across the unknown boundary $\delta(x)$ by the condition of continuous pressure.

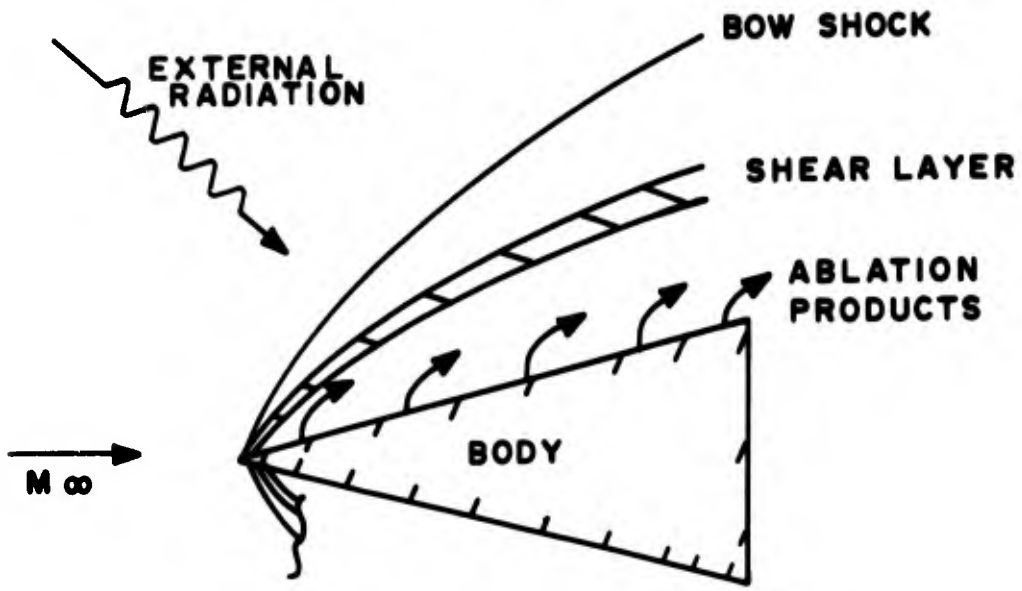
BOW SHOCK
EXTERNAL RADIATION
SHEAR LAYER
ABLATION PRODUCTS
BODY
M ∞

Fig C1

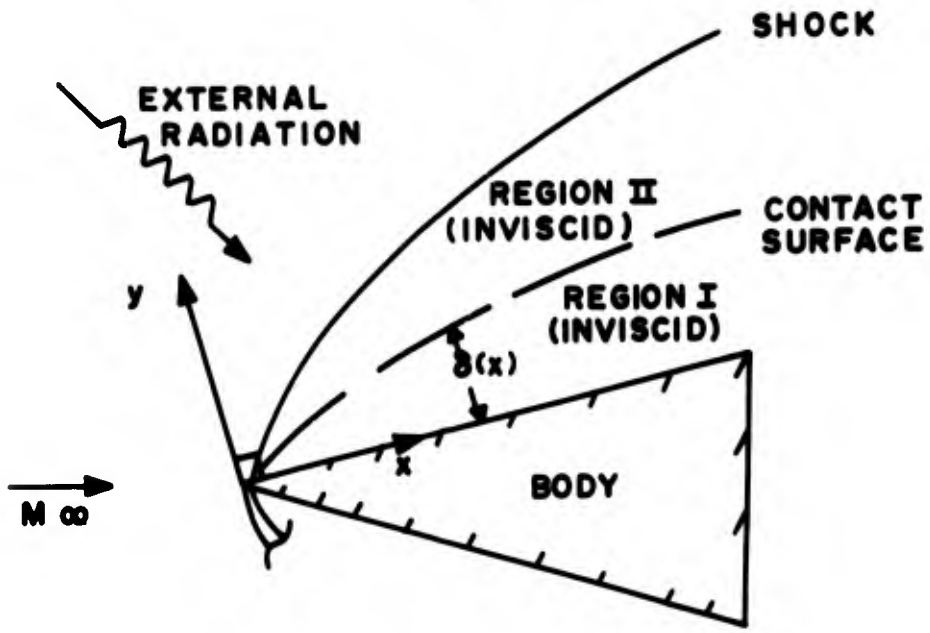
SHOCK
EXTERNAL RADIATION
REGION II (INVISCID)
CONTACT SURFACE
REGION I (INVISCID)
y
δ(x)
x
BODY
M ∞

Fig C2